Cavity-Mediated Entanglement of Parametrically Driven Spin Qubits via Sidebands

V. Srinivasa[1,*] J. M. Taylor,[2,3,4] and J. R. Petta[5,6]

[1]*Department of Physics, University of Rhode Island, Kingston, Rhode Island 02881, USA*

[2]*Joint Quantum Institute, University of Maryland, College Park, Maryland 20742, USA*

[3]*Joint Center for Quantum Information and Computer Science, University of Maryland, College Park, Maryland 20742, USA*

[4]*National Institute of Standards and Technology, Gaithersburg, Maryland 20899, USA*

[5]*Department of Physics and Astronomy, University of California—Los Angeles, Los Angeles, California 90095, USA*

[6]*Center for Quantum Science and Engineering, University of California—Los Angeles, Los Angeles, California 90095, USA*

We consider a pair of quantum dot-based spin qubits that interact via microwave photons in a superconducting cavity and that are also parametrically driven by separate external electric fields. For this system, we formulate a model for spin qubit entanglement in the presence of mutually off-resonant qubit and cavity frequencies. We show that the sidebands generated via the driving fields enable highly tunable qubit-qubit entanglement using only ac control and without requiring the qubit and cavity frequencies to be tuned into simultaneous resonance. The model we derive can be mapped to a variety of qubit types, including detuning-driven one-electron spin qubits in double quantum dots and three-electron resonant exchange qubits in triple quantum dots. The high degree of nonlinearity inherent in spin qubits renders these systems particularly favorable for parametric drive-activated entanglement. We determine multiple common resonance conditions for the two driven qubits and the cavity and identify experimentally relevant parameter regimes that enable the implementation of entangling gates with suppressed sensitivity to cavity photon occupation and decay. The parametrically driven sideband resonance approach that we describe provides a promising route toward scalability and modularity in spin-based quantum information processing through drive-enabled tunability that can also be implemented in micromagnet-free electron and hole systems for spin-photon coupling.

I. INTRODUCTION

Scaling to many-qubit systems represents a current challenge in the implementation of quantum information processing [1,2] due to the highly complex electronics required to control even a few qubits in most realizations, combined with the need to minimize dissipation of quantum information into the environment. One approach to addressing this challenge is provided by modularity [3–8], which enables scalability by linking existing, relatively well-controlled, and locally optimized few-qubit modules via robust long-range interactions. For semiconductor spin qubits, which represent a promising quantum information processing platform [9–19], such long-range interactions can be achieved by coupling spins to photons in a microwave cavity using the approach of circuit quantum electrodynamics (cQED) [19–28].

Building on the promise of long coherence times for spins in silicon [15–17,29–31], strong spin-photon coupling [32–36] as well as coherent photon-mediated interaction of two single-electron silicon spin qubits [37,38] have now been achieved. While these results provide a path to scalability for spin-based quantum information processing, tuning and scaling challenges remain for applying this approach to more than two qubits. For resonant cavity-mediated qubit-qubit coupling [37], all qubit frequencies must be tuned into simultaneous resonance with the cavity frequency, and the micromagnets required in silicon for achieving sufficient spin-charge coupling must be

*Corresponding author: vsriniv@uri.edu

precisely positioned for each qubit. In the standard dispersive approach to cavity-mediated coupling [21,23, 35,38–40], these constraints are partially relaxed as the cavity virtually mediates the interaction and its frequency is distinct from those of the qubits. However, an entangling interaction between the two qubits still requires their (cavity-shifted) frequencies to be tuned into mutual resonance.

To allow for increased flexibility in achieving qubit-qubit entanglement, off-resonant coupling approaches have been developed for cQED systems with superconducting qubits [23,26,41–47] and related two-qubit gates have also recently been explored in the context of semiconductor qubits [48–54]. These approaches enable qubits to be fixed at optimal operation points where decoherence is minimized, while interactions are activated via external microwave driving of either the coupling or one or more qubits. In particular, driving specific system parameters can generate interactions via effective resonances between intrinsically off-resonant elements by virtue of drive-induced sideband frequencies. Such a parametric approach for realizing entangling gates has been investigated and implemented in a variety of forms in superconducting qubit systems [26,46,47,55–61].

In this work, we consider a pair of qubits based on electron spins in quantum dots that interact via microwave photons in a superconducting cavity and that are also parametrically driven by classical external electric fields (Fig. 1). For this system, we formulate a model for entanglement between the two qubits that incorporates mutually off-resonant qubit and cavity frequencies and makes use of the Mollow triplet sidebands of the driven qubits [62,63] to effectively provide multiple qubit transition frequencies for cavity-mediated coupling. This approach enables highly tunable qubit-cavity photon interactions and qubit-qubit entanglement using ac control through the applied driving fields, without requiring dc tuning of the qubit frequencies. The spin qubits can therefore be fixed at optimal operation points that allow for maximal coherence times. The model we develop can be mapped to a variety of qubit types. Here, we illustrate this mapping for both single-electron spin qubits in double quantum dots [64,65] and three-electron resonant exchange (RX) qubits in triple quantum dots [66,67] in the driven resonant regime [68].

We determine common resonance conditions for the two driven qubits and the cavity and identify parameters for implementing multiple entangling gates. In contrast to the sideband-based gates obtained for the driven resonant regime in prior work [68,69], entangling gates do not require sequences of multiple sideband pulses and additionally exhibit suppressed sensitivity to cavity photon occupation, as we verify through two-qubit fidelity calculations. The enhanced spectral flexibility inherent in the approach that we describe provides a promising route toward scalability and modularity in spin-based
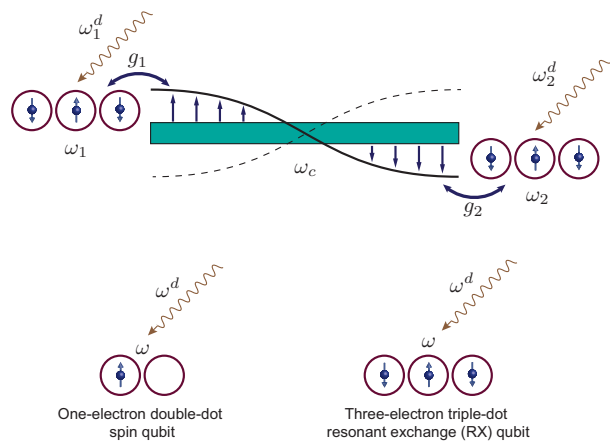

FIG. 1. Schematic illustration of a system for cavity-mediated coupling of two parametrically driven quantum dot spin qubits via sidebands. The qubits have transition frequencies ω_1 and ω_2 and are coupled to the fundamental mode of a microwave transmission line resonator (cavity), which has frequency ω_c, with strengths g_1 and g_2, respectively. The qubits are also driven by external microwave fields with frequencies ω_1^d and ω_2^d. The approach in this work can be applied to multiple types of qubits that can be sinusoidally driven, including one-electron spin qubits in double dots and three-electron resonant exchange (RX) qubits in triple dots.

quantum information processing through drive-enabled tunable entanglement that can also be implemented in micromagnet-free systems for spin-photon coupling [34–36].

II. THEORETICAL FRAMEWORK

We now develop a general theoretical description of the sideband-based cavity-mediated entangling gates between driven qubits discussed in this work. To illustrate the approach in more concrete terms, we consider two specific types of quantum dot-based electron spin qubits for which strong spin-photon coupling has been realized (Fig. 1 and Appendix A): (1) one-electron spin qubits in double quantum dots with micromagnets for spin-charge coupling [32,33,38,64]; and (2) three-electron RX qubits in triple quantum dots, which couple directly to photons through their intrinsic electric dipole moments [34,35,66–68,70]. Both types of qubits, as well as several other classes of spin qubits, such as two-electron singlet-triplet qubits [71–76], quantum dot hybrid qubits [77], and hole spin qubits in silicon and germanium double quantum dots [36,78], can be manipulated electrically by parametrically driving the detuning ϵ_j between the (outer) two dots of qubit j [65–67,79]. We write this driving field as

$$\epsilon_j(t) \equiv \epsilon_{0,j} + 2\mathcal{F}_j \cos\left(\omega_j^d t + \phi_j'\right) \tag{1}$$

in terms of a dc operation point $\epsilon_{0,j}$, as well as the amplitude $2\mathcal{F}_j$, frequency ω_j^d, and phase ϕ_j' of an ac drive that

sinusoidally modulates the detuning about $\epsilon_{0,j}$ as a function of time. Here, we fix the qubits at the "sweet-spot" detuning operation points $\epsilon_{0,j} = 0$ for $j = 1, 2$, where the first derivative of the qubit frequency vanishes for both one-electron spin and symmetric RX qubits, enabling leading-order protection from charge noise [64–67,79–85]. The operation point $\epsilon_{0,j} = 0$ also maximizes the effective spin-photon coupling strength for one-electron spin qubits [65,79], while optimization of the RX qubit-photon coupling strength involves multiple parameters (for more details, see Appendix A). In what follows, all sums are over the qubit index $j = 1, 2$ unless otherwise noted.

As shown in Appendix A, for both one-electron spin qubits and RX qubits driven according to Eq. (1), the system Hamiltonian including the cavity and driving fields with $\epsilon_{0,j} = 0$ can be written in the qubit basis as ($\hbar = 1$)

$$H_p \equiv \omega_c a^\dagger a + \sum_j \frac{\omega_j}{2} \sigma_j^z + \sum_j g_j \sigma_j^x \left(a + a^\dagger\right)$$
$$+ \sum_j 2\Omega_j \cos\left(\omega_j^d t + \phi_j\right) \sigma_j^x, \qquad (2)$$

where $a^\dagger$ and a are photon creation and annihilation operators for the fundamental mode of the cavity with frequency ω_c, σ_j^α with $\alpha = x, y, z$ and $\sigma_j^z \equiv |1\rangle_j \langle 1| - |0\rangle_j \langle 0|$ are Pauli operators and ω_j is the transition frequency for spin qubit j, g_j is the strength of the coupling between spin qubit j and photons in the fundamental cavity mode, and $2\Omega_j$ is the effective driving amplitude for spin qubit j. We see from Eq. (2) that, for both types of qubits, the detuning drive [Eq. (1)] acting on the electron charge degrees of freedom is translated into an effective transverse (σ_x) drive on the qubit. Note that we have redefined the phases ϕ_j of the drives with respect to Eq. (1) to take into account sign changes occurring in the derivation of H_p (for details, see Appendix A).

To derive sideband-mediated entangling interactions from Eq. (2), we first transform H_p to a frame rotating at the frequencies of both drives and the cavity via

$$U_1 = e^{-it\left(\omega_c a^\dagger a + \sum_j \omega_j^d \sigma_j^z / 2\right)}, \qquad (3)$$

which is equivalent to an interaction picture for resonant driving of the qubits, $\omega_j^d = \omega_j$. Defining the cavity-drive detunings $\Delta_j \equiv \omega_c - \omega_j^d$ and the qubit-drive detunings $\delta_j \equiv \omega_j - \omega_j^d$, and making a rotating wave approximation for $\left|\Delta_j\right| \ll \omega_c + \omega_j^d, 2\omega_j^d$, we drop rapidly oscillating

terms $\sim e^{\pm i\left(\omega_c + \omega_j^d\right)t}$ and $\sim e^{\pm 2i\omega_j^d t}$ and find

$$H_p^{\mathrm{rf}} \equiv U_1^\dagger H_p U_1 - i U_1^\dagger \dot{U}_1$$
$$\approx H_0 + V(t),$$
$$H_0 \equiv \sum_j \frac{\delta_j}{2} \sigma_j^z + \sum_j \Omega_j \left(e^{-i\phi_j} \sigma_j^+ + e^{i\phi_j} \sigma_j^-\right),$$
$$V(t) \equiv \sum_j g_j \left(e^{-i\Delta_j t} \sigma_j^+ a + e^{i\Delta_j t} \sigma_j^- a^\dagger\right), \qquad (4)$$

where we assume that $g_j \ll 2\Omega_j$ and take $V(t)$ as a time-dependent perturbation to the other terms in Eq. (4).

We initially take the limit $g_j \to 0$ and diagonalize H_0. Choosing the phases of the driving fields to be $\phi_j = 0$ for $j = 1, 2$ to simplify the analysis, we find that

$$H_0 = \sum_j \frac{\delta_j}{2} \sigma_j^z + \sum_j \Omega_j \sigma_j^x$$
$$\equiv \sum_j \frac{W_j}{2} \left(\cos\theta_j \sigma_j^z + \sin\theta_j \sigma_j^x\right), \qquad (5)$$

where, for convenience, we have re-expressed H_0 in terms of W_j and θ_j in the last line of Eq. (5), which serve to redefine the Pauli operators $\sigma_j^z \equiv |e\rangle_j \langle e| - |g\rangle_j \langle g|$ and σ_j^x in terms of the dressed-qubit basis $\{|e\rangle_j, |g\rangle_j\}$. We can then diagonalize this Hamiltonian via a rotation around the y axis for each qubit, described by

$$U_q = e^{-i\sum_j \theta_j \sigma_j^y / 2} \qquad (6)$$

where $\tan\theta_j = 2\Omega_j / \delta_j$, which yields

$$H_{0,q} \equiv U_q^\dagger H_0 U_q$$
$$= \sum_j \frac{W_j}{2} \sigma_j^z \qquad (7)$$

with the dressed-qubit frequencies $W_j \equiv \sqrt{\delta_j^2 + 4\Omega_j^2}$. Applying the same rotation U_q [Eq. (6)] to the qubit-cavity coupling perturbation $V(t)$ then yields the full Hamiltonian $H_q \equiv H_{0,q} + V_q(t)$ in the dressed-qubit basis, where $V_q(t) \equiv U_q^\dagger V(t) U_q$.

Finally, we transform to a second frame rotating at the dressed-qubit frequencies W_j for the driven qubits via

$$U_2 = e^{-i\sum_j W_j \sigma_j^z / 2}, \qquad (8)$$

which is equivalent to the interaction picture with respect to $H_{0,q}$ [see Eq. (7)]. In this frame, we find the Hamiltonian

$$V_I(t) \equiv U_2^\dagger H_q U_2 - i U_2^\dagger \dot{U}_2$$
$$= A(t) a^\dagger + A^\dagger(t) a. \qquad (9)$$

In Eq. (9), we have defined

$$A(t) \equiv \sum_j A_j$$

$$\equiv \sum_j \frac{g_j}{2} e^{i\Delta_j t} \left[\sin\theta_j \sigma_j^z - \left(1 - \cos\theta_j\right) e^{iW_j t} \sigma_j^+ \right.$$

$$\left. + \left(1 + \cos\theta_j\right) e^{-iW_j t} \sigma_j^- \right], \tag{10}$$

which represents a sum of time-dependent qubit operators. We note that $A(t)$, and therefore $V_I(t)$, have the three characteristic frequencies Δ_j and $\Delta_j \pm W_j$ for qubit j, which correspond to the Mollow triplet frequencies [62] consisting of the center and sideband frequencies of each driven qubit. In the present case, these frequencies are uniformly shifted by the cavity frequency ω_c due to the rotating-frame transformation U_1 [Eq. (3)]. Driving the qubits on resonance such that $\omega_j^d = \omega_j$ gives $\delta_j = 0$ and $W_j = 2\Omega_j$, so that $\sin\theta_j = 1$ and $\cos\theta_j = 0$. In this case, Eq. (10) reduces to

$$A_r(t) \equiv \sum_j \frac{g_j}{2} \left[e^{i\Delta_j t} \sigma_j^z - e^{i(\Delta_j + 2\Omega_j)t} \sigma_j^+ + e^{i(\Delta_j - 2\Omega_j)t} \sigma_j^- \right], \tag{11}$$

and we find that the three characteristic frequencies for driven qubit j become $\Delta_j, \Delta_j \pm 2\Omega_j$.

In order to determine the gate operations generated by the time-dependent Hamiltonian $V_I(t)$ in Eq. (9), we use the Magnus expansion [86] up to second order to approximate the time-evolution operator. For $g_j \ll W_j$ such that $\lambda \equiv g_j/W_j$ is a small parameter, we write $U(\tau) \approx e^{-iH_{\text{eff}}\tau}$, where $H_{\text{eff}}(\tau) = \lambda\bar{H}_1(\tau) + \lambda^2\bar{H}_2(\tau)$ represents an effective Hamiltonian to $O(\lambda^2)$ with

$$\lambda\bar{H}_1(\tau) \equiv \frac{1}{\tau} \int_0^\tau dt\, V_I(t), \tag{12}$$

$$\lambda^2\bar{H}_2(\tau) \equiv \frac{1}{2i\tau} \int_0^\tau dt \int_0^t dt'\, \left[V_I(t), V_I(t')\right]. \tag{13}$$

We first consider the term $\lambda\bar{H}_1(\tau)$. From Eqs. (9) and (10), we see that the integral in Eq. (12) is evaluated via the corresponding integrals of $A(t)$ and its Hermitian conjugate. The first-order term in the effective Hamiltonian is then given by

$$\lambda\bar{H}_1(\tau) = \sum_j \frac{g_j}{2} \left[f\left(\Delta_j\right) \sin\theta_j \sigma_j^z \right.$$

$$- f\left(\Delta_j + W_j\right)\left(1 - \cos\theta_j\right)\sigma_j^+$$

$$\left. + f\left(\Delta_j - W_j\right)\left(1 + \cos\theta_j\right)\sigma_j^- \right] a^\dagger + \text{H.c.}, \tag{14}$$

where we have defined the integral

$$f(\mu) \equiv \frac{1}{\tau} \int_0^\tau dt\, e^{i\mu t} \tag{15}$$

with frequencies $\mu = \Delta_j, \Delta_j \pm W_j$. The first-order term $\lambda\bar{H}_1(\tau)$ describes the direct $(\sim g_j)$ interaction of each qubit with the cavity and includes both red $(\sim\sigma_j^+ a, \sigma_j^- a^\dagger)$ and blue $(\sim\sigma_j^+ a^\dagger, \sigma_j^- a)$ sideband terms. These interaction terms can be used to generate entanglement via sequences of multiple sideband pulses [23,42,43,68,69,87].

We now set $\Delta_j = p_j\eta$ and $W_j = q_j\eta$ with p_j, q_j integers and $\eta \equiv 2\pi/\tau$. We also assume $\mu \neq 0$. In this case, we find that $\mu = r_j\eta$ with $r_j = p_j, p_j \pm q_j \neq 0$ also an integer, so that all integrals $f(\mu)$ in Eq. (14) vanish and $\lambda\bar{H}_1(\tau) = 0$. Thus, when Δ_j and W_j are both integer multiples of the same frequency η, we can completely eliminate the first-order sideband interaction terms [Eq. (14)] from $H_{\text{eff}}(\tau)$.

To $O(\lambda^2)$, the effective interaction Hamiltonian generating the gate operation is now given entirely by the second-order term

$$H_{\text{eff}}(\tau) = \lambda^2\bar{H}_2(\tau) = \frac{1}{2i\tau} \int_0^\tau dt \int_0^t dt'\, \left[V_I(t), V_I(t')\right]. \tag{16}$$

Using Eqs. (9) and (10), we can write the commutator in Eq. (16) as

$$\left[V_I(t), V_I(t')\right] = \left[V_I, V_I'\right]_1 + \left[V_I, V_I'\right]_2,$$

$$\left[V_I, V_I'\right]_1 \equiv \sum_j \left\{ \left[A_j, A_j'\right] a^{\dagger 2} + \left[A_j^\dagger, A_j'^\dagger\right] a^2 \right.$$

$$\left. + \left(\left[A_j, A_j'^\dagger\right] + \left[A_j^\dagger, A_j'\right]\right) a^\dagger a \right\},$$

$$\left[V_I, V_I'\right]_2 \equiv A^\dagger A' - A'^\dagger A, \tag{17}$$

where $\left[V_I, V_I'\right]_1$ contains terms involving only one-qubit operators and $\left[V_I, V_I'\right]_2$ contains all two-qubit operator terms along with some additional one-qubit operator terms, as we show below. We note in particular that $\left[V_I, V_I'\right]_2$ does not involve any photon operators.

The form of the qubit-qubit interaction terms in the effective Hamiltonian, and thus the generated two-qubit gate, is determined by $\left[V_I, V_I'\right]_2 = A^\dagger A' - A'^\dagger A$. For $j, k = 1, 2$, we can write this commutator as

$$\left[V_I, V_I'\right]_2 = A^\dagger A' - A'^\dagger A$$

$$= \sum_{j,k} \left(A_j^\dagger A_k' - A_j'^\dagger A_k\right)$$

$$= \sum_j \left(A_j^\dagger A_j' - A_j'^\dagger A_j\right)$$

$$+ A_1^\dagger A_2' - A_1'^\dagger A_2 + A_2^\dagger A_1' - A_2'^\dagger A_1. \tag{18}$$

The terms $A_j^\dagger A_j' - A_j'^\dagger A_j$ in $[V_I, V_I']_2$ lead to one-qubit terms in $H_{\text{eff}}(\tau)$, while the qubit-qubit interaction terms arise entirely from the last line of Eq. (18). In Appendix B, we show that for $\Delta_j, W_j \neq 0$ and $W_j \neq |\Delta_j|, |2\Delta_j|$, the complete one-qubit contribution to $H_{\text{eff}}(\tau)$ appearing at second order and originating from $[V_I, V_I']_1$ and $[V_I, V_I']_2$ reduces to

$$\Lambda = -\sum_j g_j^2 \left[\frac{\delta_j^2 + 2\Delta_j \delta_j + W_j^2}{2W_j \left(\Delta_j^2 - W_j^2 \right)} \right] \sigma_j^z \left(a^\dagger a + \frac{1}{2} \right). \tag{19}$$

These terms represent parametric driving-induced dispersive shifts that can be tuned via the drive amplitudes and frequencies and are well defined in the absence of decay provided that $W_j \neq |\Delta_j|$. Such shifts can be harnessed for drive-tunable qubit measurement [88]. Two specific cases of interest are $\delta_j = 0$ and $\delta_j \neq 0$, corresponding to resonant and off-resonant driving of the qubits, respectively. For $\delta_j = 0$ and $W_j \neq 0$, we find from Eq. (19) that $\Lambda \neq 0$ and the dispersive-shift terms persist. In this case, the qubit frequencies are $W_j = 2\Omega_j$ and the dispersive-shift terms in Eq. (19) become

$$\Lambda_r = \sum_j \chi_j \sigma_j^z \left(a^\dagger a + \frac{1}{2} \right),$$

$$\chi_j \equiv -\frac{g_j^2 \Omega_j}{\Delta_j^2 - 4\Omega_j^2}. \tag{20}$$

As we show in Appendix D for multiple example cases, the effects of Λ_r on the dynamics for $\delta_j = 0$ can effectively be eliminated in specific situations of interest by an appropriate choice of parameters and operation times. On the other hand, for $\delta_j \neq 0$, we can choose Δ_j and W_j such that $\Lambda = 0$ (for further details, see Appendix D). The effective Hamiltonian $H_{\text{eff}}(\tau)$ then consists purely of qubit-qubit interaction terms, which arise from the terms with $j \neq k$ in Eq. (18).

III. DRIVE-TAILORED ENTANGLING GATES VIA SIDEBAND RESONANCES

We next focus on the qubit-qubit interaction terms in $H_{\text{eff}}(\tau)$, which are given by

$$V_{qq}(\tau) \equiv \frac{1}{2i\tau} \int_0^\tau dt \int_0^t dt' \left(-A_1 A_2'^\dagger + A_1' A_2^\dagger - \text{H.c.} \right). \tag{21}$$

Using Eqs. (10) and (B3) in Appendix B to write Eq. (21) in terms of functions $h(\mu_1, \mu_2)$, $h(\mu_2, \mu_1)$, and their complex conjugates, we can identify resonance conditions

$\mu_1 = \mu_2$ that each give rise to specific qubit-qubit terms in $V_{qq}(\tau)$. Since $\mu_1 \in \{\Delta_1, \Delta_1 + W_1, \Delta_1 - W_1\}$ and $\mu_2 \in \{\Delta_2, \Delta_2 + W_2, \Delta_2 - W_2\}$, there are nine resonance conditions. Each condition corresponds to resonance between a center or sideband frequency of qubit 1 and a center or sideband frequency of qubit 2. These conditions and the corresponding qubit-qubit terms appearing in the effective Hamiltonian $H_{\text{eff}}(\tau)$ are derived in Appendix C and summarized in Table I, where we have defined $\Delta_j^\pm \equiv \Delta_j \pm W_j$.

We now specifically consider the case of resonant qubit driving ($\delta_j = 0$ or $\omega_j^d = \omega_j$), so that $W_j = 2\Omega_j$. The Hamiltonian for this case is given by $V_I(t)$ [Eq. (9)] with $A(t) = A_r(t)$ as given in Eq. (11). The characteristic frequencies are therefore $\Delta_j, \Delta_j + 2\Omega_j$, and $\Delta_j - 2\Omega_j$, corresponding to center, red sideband, and blue sideband frequencies, respectively, for driven qubit j (shifted with respect to the cavity frequency ω_c). Assuming that we choose parameters such that the effects of the drive-induced dispersive-shift terms Λ_r in Eq. (20) can be neglected (for details, see Appendix D), the evolution generated by the effective Hamiltonian $H_{\text{eff}}(\tau)$ reduces to that generated by the qubit-qubit interaction $V_{qq}(\tau)$ in Eq. (21). Thus, in what follows, we consider only the dynamics generated by $V_{qq}(\tau)$.

For each resonance condition, Table I gives the form of the interaction $V_{qq} \equiv V_{qq}(\tau)$ for resonant qubit driving (second-to-last column), assuming that the dressed-qubit frequencies W_1 and W_2 satisfy the associated constraints (third column). These constraints are based on Eq. (B3) and are obtained for each resonance condition by applying the condition $\mu_1 \neq \mu_2$ to the remaining resonance conditions in Table I, so that all qubit-qubit interaction terms except for the specified interaction V_{qq} vanish (see Appendix C). We define a corresponding ideal two-qubit operation generated by V_{qq} as $U_m \equiv U(\tau_m) = e^{-iV_{qq}\tau_m}$, where $\tau_m \equiv m\tau = 2\pi m/\eta$ with $m = 0, 1, 2, \dots$ represents the corresponding gate time and is an integer multiple of τ. By adjusting the drive amplitudes $2\Omega_j$ and frequencies ω_j^d to tune to a particular resonance condition and set W_1 and W_2 appropriately, it is then possible to select desired qubit-qubit interaction terms and two-qubit entangling gates. Examples of universal entangling gates are given in the last column of Table I. The drives can also be used to switch off a given interaction by tuning the sidebands away from the corresponding resonance condition. We emphasize that: (1) multiple two-qubit interaction terms exist even with mutually off-resonant frequencies (i.e., for $j \neq k$, $\omega_j \neq \omega_k \neq \omega_c$); and (2) the cavity photon operators $a, a^\dagger$ do not appear explicitly in V_{qq}, suggesting suppression of errors due to cavity photon decay in the sideband-based entangling gate approach we propose in this work. Our analysis of expected gate performance in Sec. IV quantitatively demonstrates the presence of this suppressed cavity photon sensitivity.

TABLE I. Resonance conditions, corresponding qubit-qubit interaction terms $V_{qq} \equiv V_{qq}(\tau)$ [Eq. (21)] in the second-order effective Hamiltonian [Eq. (16)], and generated universal entangling gates for resonant driving of the qubits ($\delta_j = 0$ for $j = 1, 2$), such that $W_j = 2\Omega_j$. The coupling strength for each interaction is given by $\mathcal{J} = g_1 g_2 / 4\Delta$, where for notational simplicity we use Δ to represent the distinct resonant detuning $\Delta_{(R)}$ for each resonance condition R, i.e., $\Delta \equiv \Delta_{(R)}$, where $\Delta_{(R)}$ is defined in the second column [$\Delta_{(1)} \equiv \Delta_1 = \Delta_2, \Delta_{(2)} \equiv \Delta_1 = \Delta_2^+, \ldots$] with $\Delta_j^\pm \equiv \Delta_j \pm W_j$ (for details, see Appendix C).

R	Resonance condition $[\Delta \equiv \Delta_{(R)}]$	Constraints	Interaction V_{qq} $(\delta_1 = \delta_2 = 0)$	Entangling gate
1	$\Delta_1 = \Delta_2$	$W_1 \neq \pm W_2$	$-2\mathcal{J}\sigma_1^z \sigma_2^z$	Controlled-phase (U_φ)
2	$\Delta_1 = \Delta_2^+$	$W_1 \neq \pm W_2, \pm 2W_2$	$\mathcal{J}\sigma_1^z \sigma_2^x$	CNOT
3	$\Delta_1 = \Delta_2^-$	$W_1 \neq \pm W_2, \pm 2W_2$	$-\mathcal{J}\sigma_1^z \sigma_2^x$	CNOT
4	$\Delta_1^+ = \Delta_2$	$W_1 \neq \pm W_2, \pm W_2/2$	$\mathcal{J}\sigma_1^x \sigma_2^z$	CNOT
5	$\Delta_1^- = \Delta_2$	$W_1 \neq \pm W_2, \pm W_2/2$	$-\mathcal{J}\sigma_1^x \sigma_2^z$	CNOT
6	$\Delta_1^+ = \Delta_2^+$	$W_1 \neq W_2, 2W_2, W_2/2$	$-\mathcal{J}\left(\sigma_1^+ \sigma_2^- + \sigma_1^- \sigma_2^+\right)$	iSWAP ($U_{i\text{SW}}$)
7	$\Delta_1^- = \Delta_2^-$	$W_1 \neq W_2, 2W_2, W_2/2$	$-\mathcal{J}\left(\sigma_1^+ \sigma_2^- + \sigma_1^- \sigma_2^+\right)$	iSWAP ($U_{i\text{SW}}$)
8	$\Delta_1^+ = \Delta_2^-$	$W_1 \neq -W_2, -2W_2, -W_2/2$	$\mathcal{J}\left(\sigma_1^+ \sigma_2^+ + \sigma_1^- \sigma_2^-\right)$	Double-excitation ($U_{i\text{DE}}$)
9	$\Delta_1^- = \Delta_2^+$	$W_1 \neq -W_2, -2W_2, -W_2/2$	$\mathcal{J}\left(\sigma_1^+ \sigma_2^+ + \sigma_1^- \sigma_2^-\right)$	Double-excitation ($U_{i\text{DE}}$)

To more concretely illustrate the approach, we now consider the effective qubit-qubit interaction and entangling gates generated between resonantly driven qubits ($\delta_j = 0$, $W_j = 2\Omega_j$) for the specific resonance conditions 7 and 9 in Table I. First, we consider $\Delta_1^- = \Delta_2^-$ (resonance condition 7), which is equivalent to $\Delta_1 - W_1 = \Delta_2 - W_2$. As described in Appendix C, the resonance condition can also be written as $\omega_1 + 2\Omega_1 = \omega_2 + 2\Omega_2$ for resonantly driven qubits and describes resonance between the blue sidebands of both qubits [Fig. 2(a)]. Setting $\Delta_j = p_j \eta$ and $W_j = q_j \eta$ with p_j, q_j integers leads to the equivalent condition $p_1 - q_1 = p_2 - q_2$. We also define the integer $w \equiv p_1 - q_1 = p_2 - q_2$ such that $\Delta \equiv \Delta_1^- = \Delta_2^- = w\eta$. From Table I, the constraints associated with resonance condition 7 are $W_1 \neq W_2, 2W_2, W_2/2$. Assuming that these constraints are satisfied, the qubit-qubit interaction takes the form $V_{qq} = -\mathcal{J}\left(\sigma_1^+ \sigma_2^- + \sigma_1^- \sigma_2^+\right)$ with coupling strength $\mathcal{J} \equiv g_1 g_2 / 4\Delta$.

This interaction can be used to generate the iSWAP gate, which together with single-qubit rotations constitutes a universal set of quantum gates [89] and also represents a key element of recently proposed improvements to the implementation of quantum error correction using the surface code [90]. Since V_{qq} is independent of the photon operators $a, a^\dagger$, $U_m \equiv e^{-iV_{qq}\tau_m}$ acts nontrivially only on the qubits and we can work in a subspace of fixed photon number n. Thus, we now project all states and operators into the subspace defined by $P_n \equiv |n\rangle \langle n|$. For notational simplicity, we use U_m to denote the evolution operators within the n-photon two-qubit subspace $\{|ee, n\rangle, |eg, n\rangle, |ge, n\rangle, |gg, n\rangle\}$ in the remainder of this work unless otherwise specified. Defining $\Sigma_x \equiv |eg\rangle \langle ge| + |ge\rangle \langle eg|$ (where we have suppressed the photon-number state $|n\rangle$ for convenience), we can write $V_{qq} = -\mathcal{J}\Sigma_x$ and $U_m = e^{i\mathcal{J}\tau_m \Sigma_x}$. In the full two-qubit dressed basis $\{|ee\rangle, |eg\rangle, |ge\rangle, |gg\rangle\}$, U_m takes the form

$$U_m = \begin{pmatrix} 1 & 0 & 0 & 0 \\ 0 & \cos(\mathcal{J}\tau_m) & i\sin(\mathcal{J}\tau_m) & 0 \\ 0 & i\sin(\mathcal{J}\tau_m) & \cos(\mathcal{J}\tau_m) & 0 \\ 0 & 0 & 0 & 1 \end{pmatrix}. \quad (22)$$

In order to obtain an iSWAP gate $U_{i\text{SW}}$, we set $\tau_m = m\tau = \pi/2\mathcal{J}$. We choose the initial state $|\psi_i\rangle = |eg\rangle$ for our analysis. To cancel the dynamics due to the dispersive-shift terms in Eq. (20) for this case, we also set $\chi_1 = \chi_2$. As shown in Appendix D, both the generation of the iSWAP gate and the drive-induced dispersive shift cancellation can be achieved for resonance condition 7 by choosing parameters that satisfy the constraints in Eqs. (D9) and (D10). These relations are satisfied for multiple sets of parameters. For the analysis in this work, we choose the set of parameters shown for resonance condition 7 in Table II. The evolution time unit in the Magnus expansion becomes $\tau = 2\pi/\eta = 20$ ns, yielding an iSWAP gate time $\tau_m = m\tau = 800$ ns. As discussed in detail in Appendix D, the ideal gate evolution generated by V_{qq} at time τ_m for resonance condition 7 and these parameters [described by a pure state $\rho_I^f(\tau_m)$] approximates well the numerical evolution directly due to Eq. (9) according to the time-dependent Schrödinger equation and in the absence of qubit and cavity decay [described by a pure state $\rho_I^{(0)}(\tau_m)$], with a fidelity $F_0 \approx 0.998$ calculated according to Eq. (D12) (we choose the subspace with $n = 0, 1, 2$ and the initial state $|\psi_i\rangle = |eg, 0\rangle$ for the numerical analysis; see Appendix D).

Resonance condition 9 in Table I is given by $\Delta \equiv \Delta_1^- = \Delta_2^+$. For resonantly driven qubits, this condition can also be written as $\omega_1 + 2\Omega_1 = \omega_2 - 2\Omega_2$ (see Appendix C) and describes resonance between the blue sideband of qubit 1 and the red sideband of qubit 2 [Fig. 2(b)]. For $\Delta_j = p_j \eta$ and $W_j = q_j \eta$, the resonance
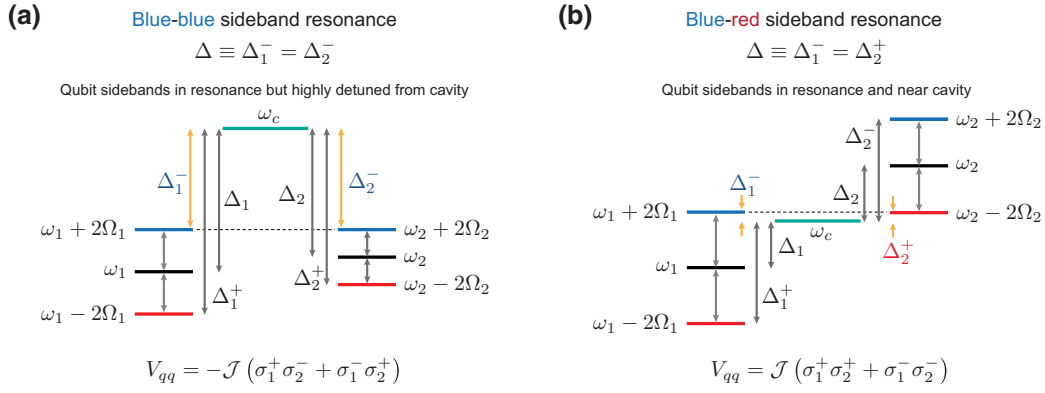
FIG. 2.   Examples of qubit-qubit interactions enabled by cavity-mediated coupling via resonant sidebands of parametrically driven qubits. (a) Blue-blue sideband resonance, described by $\Delta_1^- = \Delta_2^-$ (resonance condition 7 in Table I). The diagram shown depicts a case in which the resonant sidebands are highly detuned from the cavity frequency ω_c. (b) Blue-red sideband resonance, described by $\Delta = \Delta_1^- = \Delta_2^+$ (resonance condition 9 in Table I). The diagram depicts a case in which the resonant sidebands are near the cavity frequency ω_c. In both cases, the qubit frequencies $\omega_{1,2}$ and the cavity frequency ω_c are mutually off-resonant, i.e., $\omega_1 \neq \omega_2 \neq \omega_c$.

condition can also be expressed as $p_1 - q_1 = p_2 + q_2$. Accordingly, we now define $w \equiv p_1 - q_1 = p_2 + q_2$ such that $\Delta \equiv \Delta_1^- = \Delta_2^+ = w\eta$. Assuming that the constraints $W_1 \neq -W_2, -2W_2, -W_2/2$ associated with resonance condition 9 are satisfied (note that these constraints are always satisfied for $W_{1,2} > 0$), the qubit-qubit interaction is $V_{qq} = \mathcal{J} \left(\sigma_1^+ \sigma_2^+ + \sigma_1^- \sigma_2^- \right)$ with coupling strength $\mathcal{J} \equiv g_1 g_2 / 4\Delta$.

We again note that V_{qq} is independent of the photon operators $a, a^\dagger$ and generates the gate $U_m \equiv e^{-iV_{qq}\tau_m}$ within the n-photon subspace at time $\tau_m = m\tau$. In terms of $\Sigma_x' \equiv |ee\rangle \langle gg| + |gg\rangle \langle ee|$, we find $V_{qq} = \mathcal{J} \Sigma_x'$ and $U_m = e^{-i\mathcal{J}\tau_m \Sigma_x'}$, yielding

$$U_m = \begin{pmatrix} \cos(\mathcal{J}\tau_m) & 0 & 0 & -i\sin(\mathcal{J}\tau_m) \\ 0 & 1 & 0 & 0 \\ 0 & 0 & 1 & 0 \\ -i\sin(\mathcal{J}\tau_m) & 0 & 0 & \cos(\mathcal{J}\tau_m) \end{pmatrix} \quad (23)$$

in the full two-qubit dressed basis. The gate at $\tau_m = m\tau = -\pi/2\mathcal{J}$ is analogous to an iSWAP gate but acts in the subspace spanned by $\{|ee\rangle, |gg\rangle\}$. We denote this gate, which we refer to as the double-excitation gate, by $U_{i\mathrm{DE}}$. As the gate is related to $U_{i\mathrm{SW}}$ via a rotation of qubit 2, $U_{i\mathrm{DE}}$ together with single-qubit rotations also constitutes a universal set of quantum gates. For our analysis, we choose the initial state $|\psi_i\rangle = |ee\rangle$ and also set $\chi_1 = -\chi_2$ to cancel the dynamics due to the dispersive-shift terms in Eq. (20) (Appendix D). Simultaneous generation of the gate $U_{i\mathrm{DE}}$ and cancellation of the drive-induced dispersive shifts for resonance condition 9 is possible by choosing parameters that satisfy the constraints in Eqs. (D16) and (D17). As in the case of resonance condition 7, these relations are satisfied for multiple sets of parameters. Here, we choose the parameters specified in Table II for resonance condition 9. The evolution time unit in the Magnus expansion is

again $\tau = 2\pi/\eta = 20$ ns, yielding a gate time $\tau_m = m\tau = 200$ ns for $U_{i\mathrm{DE}}$. Using Eq. (D12) to compare the ideal gate evolution generated by V_{qq} at time τ_m for resonance condition 9 and these parameters with the numerical evolution directly due to Eq. (9) according to the time-dependent Schrödinger equation and in the absence of qubit and cavity decay again yields a fidelity $F_0 \approx 0.998$ (as described in Appendix D, we again choose the subspace with $n = 0, 1, 2$ along with the initial state $|\psi_i\rangle = |ee, 0\rangle$ for the numerical analysis). Note that the parameter values given in Table II are chosen in accordance with experimental implementations of one-electron double-dot and three-electron triple-dot spin qubits (see the descriptions and references cited for these systems in Appendix A).

We therefore find that (as reflected in the calculated values of F_0), for both resonance conditions 7 and 9 and appropriately selected parameters, the dynamics due to V_I with cavity photon operators explicitly included are well approximated by the dynamics generated by just the two-qubit interaction V_{qq}, from which cavity photon operators are absent. In Sec. IV, we show that this absence of explicit cavity photon dependence in the effective Hamiltonian is manifested in the full dynamics as suppressed sensitivity of these sideband-based entangling gates to cavity photon decay.

IV. SIDEBAND GATE PERFORMANCE IN THE PRESENCE OF QUBIT AND CAVITY DECAY

To evaluate the performance of the sideband resonance-based gates $U_{i\mathrm{SW}}$ and $U_{i\mathrm{DE}}$ and quantitatively illustrate the reduced dependence of the dynamics on cavity photons, we use a master-equation analysis and numerically calculate the fidelity with respect to the ideal dynamics for resonance conditions 7 and 9 in the presence of qubit and

TABLE II. Parameter values used in the effective interaction Hamiltonian and entangling gate analysis for resonance conditions 7 and 9 in Table I, assuming resonantly driven qubits ($\delta_j \equiv \omega_j - \omega_j^d = 0$ for $j = 1, 2$) such that $W_j = 2\Omega_j$. Each set of parameters satisfies the associated resonance condition with $W_j = 2\Omega_j = q_j \eta$, $\Delta_j \equiv \omega_c - \omega_j^d = p_j \eta$, $\Delta_j^\pm \equiv \Delta_j \pm W_j$, $\mathcal{J} = g_1 g_2 / 4\Delta$, χ_j as given in Eq. (20), and the constraints in Eqs. (D9) and (D10) [Eqs. (D16) and (D17)] for resonance condition 7 (9).

Parameter	Resonance condition 7: $\Delta \equiv \Delta_1^- = \Delta_2^-$	Resonance condition 9: $\Delta \equiv \Delta_1^- = \Delta_2^+$
q_1	7	12
q_2	4	11
p_1	20	10
p_2	17	-13
w	13	-2
m	40	10
$\eta/2\pi = 1/\tau$	0.05 GHz	0.05 GHz
$g_1/2\pi$	26 MHz	21 MHz
$g_2/2\pi$	31 MHz	23 MHz
$\omega_1/2\pi$	6 GHz	5.7 GHz
$\omega_2/2\pi$	6.15 GHz	6.85 GHz
$\omega_c/2\pi$	7 GHz	6.2 GHz
$W_1/2\pi = 2\Omega_1/2\pi$	0.35 GHz	0.6 GHz
$W_2/2\pi = 2\Omega_2/2\pi$	0.2 GHz	0.55 GHz
$\Delta_1/2\pi$	1 GHz	0.5 GHz
$\Delta_2/2\pi$	0.85 GHz	-0.65 GHz
$\Delta_1^+/2\pi$	1.35 GHz	1.1 GHz
$\Delta_1^-/2\pi$	0.65 GHz	-0.1 GHz
$\Delta_2^+/2\pi$	1.05 GHz	-0.1 GHz
$\Delta_2^-/2\pi$	0.65 GHz	-1.2 GHz
$\mathcal{J}/2\pi$	0.31 MHz	-1.25 MHz
$\chi_1/2\pi$	-0.14 MHz	1.25 MHz
$\chi_2/2\pi$	-0.14 MHz	-1.25 MHz

cavity decay. Here, we assume that dephasing in the original qubit basis with rate γ_j for qubit j and cavity photon loss with rate κ are the dominant sources of decoherence, as is relevant for silicon quantum dots [68]. We write the master equation as [23,68]

$$\dot{\rho} = -i\left[H_p, \rho\right] + \sum_j \frac{\gamma_j}{2}\left(\sigma^z \rho \sigma^z - \rho\right)$$
$$+ \frac{\kappa}{2}\left(2a\rho a^\dagger - a^\dagger a \rho - \rho a^\dagger a\right), \qquad (24)$$

with H_p given by Eq. (2). Following steps similar to those used to obtain the interaction-picture Hamiltonian V_I [Eq. (9)], we transform the master equation in Eq. (24) to the interaction picture. Moving to a rotating frame via U_1 [Eq. (3)], making a rotating wave approximation for $\left|\Delta_j\right| \ll \omega_c + \omega_j^d, 2\omega_j^d$, choosing $\phi_j = 0$, applying U_q [Eq. (6)] to change to the dressed-qubit basis, and moving to the interaction picture via U_2 [Eq. (8)] yields, after setting $\delta_j = 0$ for resonant qubit driving and dropping rapidly

oscillating terms $\sim e^{\pm 2iW_j t}$,

$$\dot{\rho}_I = -i[V_I, \rho_I] + \sum_j \frac{\gamma_j}{2}\left(\sigma_j^+ \rho_I \sigma_j^- + \sigma_j^- \rho_I \sigma_j^+ - \rho_I\right)$$
$$+ \frac{\kappa}{2}\left(2a\rho_I a^\dagger - a^\dagger a \rho_I - \rho_I a^\dagger a\right), \qquad (25)$$

where $\rho_I \equiv U_2^\dagger U_q^\dagger U_1^\dagger \rho U_1 U_q U_2$. Equation (25) is the master equation describing the dynamics in the interaction picture (we find that retaining the rapidly oscillating terms dropped in the derivation of this equation does not significantly modify the quantitative results). For the numerical calculations, we again work in the photon subspace with $n = 0, 1, 2$ and set $\gamma_1 = \gamma_2 \equiv \gamma$ for simplicity. To analyze the effects of qubit and cavity decay on the performance of the entangling gates, we calculate the fidelity [91]

$$F(\tau_m) \equiv \text{Tr}\left[\rho_I^{(0)}(\tau_m)\, \rho_I(\tau_m)\right], \qquad (26)$$

where $\rho_I(\tau_m)$ denotes the final state at time τ_m for the evolution obtained by numerically integrating Eq. (25) and $\rho_I^{(0)}(\tau_m)$ denotes the final state for the ideal evolution given by $\gamma = \kappa = 0$ [note that this fidelity is distinct from F_0 given in Eq. (D12)]. We calculate this fidelity as a function of γ and κ for the resonance conditions 7 and 9 using the parameter sets in Table II and the initial states chosen above for the ideal gates U_{iSW} and U_{iDE}. The initial state is $\rho_I(0) = |\psi_i\rangle\langle\psi_i| = |eg, 0\rangle\langle eg, 0|$ for resonance condition 7 and $\rho_I(0) = |\psi_i\rangle\langle\psi_i| = |ee, 0\rangle\langle ee, 0|$ for resonance condition 9.

In Fig. 3, we plot the error $1 - F(\tau_m)$ for the two resonance conditions and corresponding two-qubit entangling gates. We find theoretical fidelities $F > 0.995$ for the full range of κ shown (up to $\kappa = 100$ kHz) and $\gamma \lesssim 1$ kHz ($\gamma \lesssim 10$ kHz) for resonance condition 7 (9). While γ and κ are varied over 3 orders of magnitude in both cases, the error for both resonance conditions depends more strongly on qubit decay γ than on cavity decay κ. This reduced dependence on κ is expected for the dispersive regime, in which the cavity virtually mediates the qubit-qubit interaction in the absence of direct qubit-photon interaction, and was also found in the results of Ref. [68] for the dispersive regimes relative to the driven resonant regime of cavity-mediated coupling. We note, however, that the gates derived here are based on interactions via sideband resonances, as in the driven resonant regime.

For resonance condition 7, given by $\Delta_1^- = \Delta_2^-$ [Fig. 3(a)], the resonant blue sidebands of the driven qubits are highly detuned from the cavity frequency ω_c, with $\Delta/2\pi = \Delta_1^-/2\pi = \Delta_2^-/2\pi = 0.65$ GHz [see Fig. 2(a)]. We see that the error varies over approximately 3 orders of magnitude with γ but over less than one order of magnitude with κ. The suppressed sensitivity to κ is expected given the large detuning between the qubit sidebands and
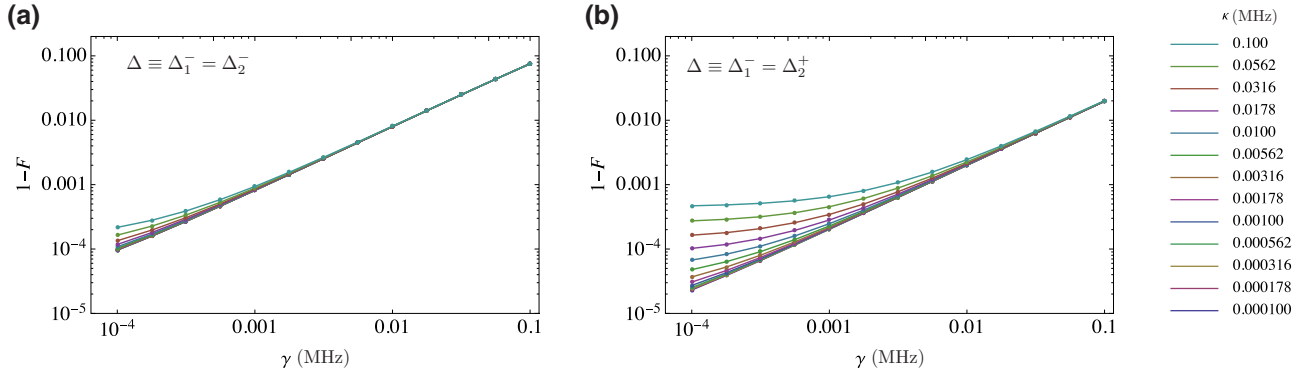
FIG. 3. Error $1 - F$ [as given by Eq. (26)] in entangling gates of duration τ_m generated by sideband-based cavity-mediated coupling of parametrically driven qubits, calculated via numerical solution of the master equation in Eq. (25) as a function of the qubit decay rate γ and cavity photon decay rate κ. (a) Error in the iSWAP gate $U_{i\text{SW}}$, generated by a blue-blue sideband resonance [Fig. 2(a)] with the initial state $|\psi_i\rangle = |eg, 0\rangle$ and parameters for resonance condition 7 given in Table II. (b) Error in the double-excitation gate $U_{i\text{DE}}$, generated by a blue-red sideband resonance [Fig. 2(b)] with the initial state $|\psi_i\rangle = |ee, 0\rangle$ and parameters for resonance condition 9 given in Table II. The lines are guides for the eye.

the cavity. On the other hand, for resonance condition 9, given by $\Delta_1^- = \Delta_2^+$ [Fig. 3(b)], the resonant sidebands—the blue sideband of qubit 1 and the red sideband of qubit 2—are close to ω_c. Here, $\Delta/2\pi = \Delta_1^-/2\pi = \Delta_2^+/2\pi = -0.1$ GHz [see Fig. 2(b)]. In this case, we see that the error again varies over approximately 3 orders of magnitude with γ, but varies over less than 2 orders of magnitude with κ. The increased variation with κ relative to resonance condition 7 reflects the smaller detuning Δ of the resonant qubit sidebands from the cavity. However, even in this case, we find that the sensitivity of the error to κ is suppressed relative to the sideband-based two-qubit gates in the driven resonant regime (compare Fig. 7 in Ref. [68]).

While the reduced sensitivity to cavity decay is consistent with the dispersive regime, it also reflects the absence of explicit cavity dependence in the effective interaction Hamiltonian V_{qq} generating the two-qubit entangling gates [Eq. (21) and Table I]. We have seen (Sec. III) that for appropriately chosen parameters, the gates generated by V_{qq} closely approximate the dynamics due to the full interaction-picture Hamiltonian V_I in Eq. (25), where a and $a^\dagger$ are explicitly present in general [see Eq. (9)]. Thus, the effective Hamiltonian we derive here illustrates that tuning the parametric drive frequencies and amplitudes with the remaining parameters set appropriately effectively enables suppression of the sensitivity to cavity decay.

V. CONCLUSIONS

In this work, we have developed an approach for achieving long-range interactions between a pair of driven spin qubits via cavity-mediated coupling combined with sideband resonances. Our approach is applicable to a variety of qubit types that can be controlled via parametric driving, including one-electron spin qubits in double quantum

dots, three-electron RX qubits in triple quantum dots, and hole spin qubits, and enables highly tunable qubit-qubit interactions that can be tailored via the driving fields. The interactions can also be switched on and off using only ac control, without requiring dc tuning of the qubits away from optimal operation points and thus allowing for improved qubit coherence relative to resonant and standard dispersive approaches for cavity-mediated qubit coupling.

We note that the approach that we describe here is based on the driving of inherently nonlinear effective two-level systems (i.e., qubits). Reducing the nonlinearity limits gate speeds and fidelities due to leakage for sufficiently large drive amplitudes and pulse bandwidths such that transitions to states outside the qubit space can be excited, in the absence of additional techniques that compensate for weak anharmonicity [92–94]. Limits to the fidelity and scalability of other drive-based off-resonant entangling approaches such as cross-resonance [44,45] and FLIC-FORQ (fixed linear couplings between fixed off-resonant qubits) [23,41] gates also exist due to small anharmonicities, required qubit frequency spacing, available bandwidth for control, and spurious interaction terms $\sim \sigma_1^z \sigma_2^z$ [26]. Spin qubits such as those considered in this work are characterized by highly nonlinear spectra in which differences of >1 GHz in transition frequencies are routinely realized, including within hybrid cQED systems [32–34], and dipole transitions are highly tunable. In addition, fluxonium superconducting qubits are designed to have high (>1 GHz) anharmonicities [95–99]. Such qubits with high inherent nonlinearities should in principle allow for greater flexibility in the choice of amplitudes, frequencies, and gate times for achieving desired high-fidelity gates via the parametric driving approach described here, without requiring the added complexity of low-anharmonicity compensation techniques.

For our driven-qubit sideband-based approach, we expect that limits on the driving amplitudes and entangling rates for implementing high-fidelity gates will instead arise primarily from the requirements that Δ_j and W_j are both integer multiples of the same frequency $\eta = 2\pi/\tau$ to eliminate the first-order interaction in Eq. (14), which sets a lower bound on τ and thus τ_m since $\eta \leq |\Delta_j|, W_j$, together with the conditions $g_j \ll W_j$ required for the validity of the effective Hamiltonian, the tuning of the drive amplitudes and frequencies to a desired resonance condition and interaction (Table I), and the constraints for eliminating other interaction terms and dynamics due to the parametric drive-induced dispersive shifts. As we have shown in this work, multiple sets of experimentally relevant [100] parameters exist for which these requirements can be simultaneously satisfied (see, e.g., Table II) in order to select desired and eliminate undesired interaction terms.

We have analyzed specific examples of sideband-based entangling gates that include a 200-ns double-excitation gate $U_{i\text{DE}}$, which is generated via a blue-red sideband resonance and does not exist for the standard dispersive regime in the absence of driving fields [21,23,35,38]. Furthermore, the rates of the entangling gates described in this work are set by $\mathcal{J} \propto \Delta^{-1}$, in contrast to the typical $\sim\Delta_j^{-1}$ scaling for standard dispersive entangling gate rates (where $\Delta_j = \omega_c - \omega_j$ for resonant qubit driving). As it is possible to have $\Delta < \Delta_j$ for multiple sideband resonance conditions (see, e.g., Table II), the corresponding entangling gates can potentially be more rapid than those in the standard dispersive regime. As the gates do not require sequences of multiple qubit-cavity sideband pulses, the potential also exists for gate speed improvements relative to the sideband-based gates in the driven resonant regime considered in prior work [68,69].

Unlike the resonant and standard dispersive approaches, realizing cavity-mediated entangling interactions via the sideband resonance method that we describe here does not rely on simultaneous mutual resonance among multiple qubit and cavity-photon frequencies. Instead, several sideband resonance conditions are available for generating entanglement between dressed qubits even with all original qubit and cavity frequencies mutually off-resonant, providing enhanced spectral flexibility. As a result, the sideband resonance-based approach represents a potential alternative to the challenging tuning required to bring single-spin-qubit frequencies into simultaneous resonance via precisely oriented micromagnets that has been essential to spin-spin coupling demonstrations in silicon to date [37,38]. In the context of extending this entangling approach to multiple qubits, we note that the spectral flexibility also enables the sideband resonances between adjacent pairs of qubits to be separated by energies $\sim 2W$. These energy separations can be tuned to large values via the frequencies and amplitudes of the drives, with $2W \gtrsim 1.1$ GHz for the example parameters given for resonance

condition 9 in Table II, and can potentially aid in minimizing crosstalk. Together with the suppressed sensitivity to cavity decay expected from our analysis of example entangling gates, these features render the approach that we present in this work favorable for scaling and promising for the implementation of modular quantum information processing with spin qubits.

ACKNOWLEDGMENTS

APPENDIX A: HAMILTONIAN FOR CAVITY-COUPLED DRIVEN SPIN QUBITS

The Hamiltonian H_p in Eq. (2) describes parametrically driven qubits coupled via the fundamental mode of microwave cavity photons and forms the basis for the sideband-based cavity-mediated entangling gates derived in this work. Here, we show how we obtain H_p for the two specific examples of driven spin qubits illustrated in Fig. 1.

1. Driven one-electron spin qubits in double quantum dots

We first consider two one-electron spin qubits in double quantum dots (DQDs) coupled via a microwave cavity [37,38]. In the following analysis, we take into account only the lowest-energy orbital level in each dot. The charge dipole of the electron in each DQD couples to the electric field of a microwave cavity photon [20], and the spin of the electron couples to the charge via spin-orbit coupling and/or a magnetic field gradient [101]. We focus on electrons occupying the lowest-energy valley states within silicon quantum dots, for which spin-charge coupling is achieved through gradient fields produced by a micromagnet [32,33,37,38,64].

Assuming coupling to only the fundamental cavity photon mode with frequency ω_c, we write the system Hamiltonian including parametrically driven detuning as

$$H_s = \omega_c a^\dagger a + H_d + \sum_{j=1,2} g_{c,j} \tau_j^z \left(a + a^\dagger \right), \quad \text{(A1)}$$

$$H_d \equiv \frac{1}{2} \sum_{j=1,2} \left[\epsilon_j(t) \tau_j^z + 2t_j \tau_j^x + B_j^z s_j^z + B_j^x \tau_j^z s_j^x \right], \quad \text{(A2)}$$

where $\tau_j^z \equiv |L\rangle_j \langle L| - |R\rangle_j \langle R|$ with $|L\rangle_j$ and $|R\rangle_j$ the lowest-energy orbital in the left and right dots of DQD j, respectively, $s_j^z \equiv |\uparrow\rangle_j \langle \uparrow| - |\downarrow\rangle_j \langle \downarrow|$ is the Pauli-z operator for the electron spin in DQD j, and the other Pauli orbital (charge) and spin operators are defined accordingly.

The remaining parameters in Eqs. (A1) and (A2) are the detuning ϵ_j between the orbital levels in the left and right dots, the interdot tunnel coupling $2t_j$, the Zeeman splittings B_j^z and B_j^x due to the net magnetic field components along the z and x axes, respectively (due to both the external and micromagnet fields [32]), and the charge-cavity coupling strength $g_{c,j}$ for DQD j.

We describe sinusoidal (ac) driving of the detuning for each DQD via Eq. (1) and choose the "sweet-spot" detuning operation points $\epsilon_{0,j} = 0$ for $j = 1, 2$ where the first derivative of the charge qubit frequency vanishes, enabling leading-order protection from charge noise [64,65,79,102]. As in the main text, all sums are over the qubit index $j = 1, 2$ unless otherwise noted. We first apply the rotation

$$U_c = e^{-i(\pi/4)\sum_j \tau_j^y} \tag{A3}$$

to the charge subspace. The system Hamiltonian H_s becomes

$$H_s' = U_c^\dagger H_s U_c$$
$$= \omega_c a^\dagger a + H_d' - \sum_j g_{c,j} \tau_j^x \left(a + a^\dagger\right)$$
$$- \sum_j \mathcal{F}_j \cos\left(\omega_j^d t + \phi_j'\right) \tau_j^x, \tag{A4}$$

$$H_d' \equiv \frac{1}{2} \sum_j \left(2t_j \tau_j^z + B_j^z s_j^z - B_j^x \tau_j^x s_j^x\right). \tag{A5}$$

Writing the transformed DQD Hamiltonian H_d' in the rotated charge-spin product basis $\{|+,\uparrow\rangle_j, |-,\downarrow\rangle_j, |+,\downarrow\rangle_j, |-,\uparrow\rangle_j\}$, where $|\pm\rangle_j = \left(|L\rangle_j \pm |R\rangle_j\right)/\sqrt{2}$ are the double-dot charge eigenstates for $\epsilon_{0,j} = 0$, reveals a block-diagonal structure with two decoupled subspaces that we label as $\mathcal{H}_{a,j}$ and $\mathcal{H}_{b,j}$ and that are spanned by $\{|+,\uparrow\rangle_j, |-,\downarrow\rangle_j\}$ and $\{|+,\downarrow\rangle_j, |-,\uparrow\rangle_j\}$, respectively [64,101].

Full diagonalization of the DQD low-energy space including spin for $\epsilon_{0,j} = 0$ is then achieved by applying

$$U_d = e^{i\sum_j \left(\Phi_{a,j} \hat{\alpha}_j^y + \Phi_{b,j} \hat{\beta}_j^y\right)/2}, \tag{A6}$$

where $\hat{\alpha}_j^y \equiv -i\left(|+,\uparrow\rangle_j \langle-,\downarrow| - |-,\downarrow\rangle_j \langle+,\uparrow|\right)$, $\hat{\beta}_j^y \equiv -i\left(|+,\downarrow\rangle_j \langle-,\uparrow| - |-,\uparrow\rangle_j \langle+,\downarrow|\right)$, and $\tan\Phi_{a(b),j} = B_j^x / \left(2t_j \pm B_j^z\right)$. For $\left|2t_j - B_j^z\right| \ll 2t_j + B_j^z$, $\tan\Phi_{a,j} \ll \tan\Phi_{b,j}$ and the degree of mixing between $|-,\downarrow\rangle_j$ and $|+,\uparrow\rangle_j$ is much smaller than that between $|-,\uparrow\rangle_j$ and $|+,\downarrow\rangle_j$. The eigenstates in the subspace $\mathcal{H}_{a,j}$ can then be approximated as [64] $|0\rangle_j \approx |-,\downarrow\rangle_j$ and $|3\rangle_j \approx |+,\uparrow\rangle_j$, and the corresponding eigenvalues (for $\hbar = 1$) are $\omega_{0,j} = -\mathcal{W}_j/2$ and $\omega_{3,j} = \mathcal{W}_j/2$ with $\mathcal{W}_j \equiv \sqrt{\left(2t_j + B_j^z\right)^2 + \left(B_j^x\right)^2}$. Setting

$\Phi_j \equiv \Phi_{b,j}$ for notational convenience, the eigenstates in the subspace $\mathcal{H}_{b,j}$ are given by

$$|1\rangle_j \equiv \sin\left(\frac{\Phi_j}{2}\right)|+,\downarrow\rangle_j + \cos\left(\frac{\Phi_j}{2}\right)|-,\uparrow\rangle_j, \tag{A7}$$

$$|2\rangle_j \equiv \cos\left(\frac{\Phi_j}{2}\right)|+,\downarrow\rangle_j - \sin\left(\frac{\Phi_j}{2}\right)|-,\uparrow\rangle_j \tag{A8}$$

and the corresponding eigenvalues are $\omega_{1,j} = -\mathcal{V}_j/2$ and $\omega_{2,j} = \mathcal{V}_j/2$ with $\mathcal{V}_j \equiv \sqrt{\left(2t_j - B_j^z\right)^2 + \left(B_j^x\right)^2}$. Defining the operators $\sigma_j^{kl} \equiv |k\rangle_j \langle l|$, we find in the DQD eigenstate basis

$$\tilde{H}_s = U_d^\dagger H_s' U_d$$
$$= \omega_c a^\dagger a + \sum_j \sum_{k=0}^{3} \omega_{k,j} \sigma_j^{kk}$$
$$- \sum_j \tilde{d}_j \left[\mathcal{F}_j \cos\left(\omega_j^d t + \phi_j'\right) + g_{c,j}\left(a + a^\dagger\right)\right], \tag{A9}$$

where we have defined

$$\tilde{d}_j \equiv U_d^\dagger \tau_j^x U_d$$
$$= d_j^{01} \sigma_j^{01} + d_j^{02} \sigma_j^{02} + d_j^{13} \sigma_j^{13} + d_j^{23} \sigma_j^{23} + \text{H.c.}, \tag{A10}$$

with $d_j^{01} = -d_j^{23} \approx \sin\left(\Phi_j/2\right)$ and $d_j^{02} = d_j^{13} \approx \cos\left(\Phi_j/2\right)$ for $\left|2t_j - B_j^z\right| \ll 2t_j + B_j^z$.

The Hamiltonian in Eq. (A9) describes each DQD in terms of a multilevel picture in which the ground state of the electron is $|0\rangle_j \approx |-,\downarrow\rangle_j$ and the highest excited state is $|3\rangle_j \approx |+,\uparrow\rangle_j$, while the dominant charge-spin character of $|1\rangle_j$ and $|2\rangle_j$ for $\epsilon_{0,j} = 0$ depends on the relative magnitudes of $2t_j$ and B_j^z [64]. To reduce the DQD description to an approximate two-level picture corresponding to a spin qubit, we choose the case $2t_j > B_j^z$ (illustrated in Ref. [64, Fig. 2(a)]) such that $|1\rangle_j \approx |-,\uparrow\rangle_j$ is the first excited state and $|2\rangle_j \approx |+,\downarrow\rangle_j$ is the second excited state for each DQD. We also assume that $\omega_{1,j} - \omega_{0,j} \ll \omega_{2,j} - \omega_{1,j}$, which is equivalent to $\left(\mathcal{W}_j - \mathcal{V}_j\right)/2\mathcal{V}_j \ll 1$, as well as $\mathcal{F}_j/\mathcal{V}_j, g_{c,j}/\mathcal{V}_j \ll 1$. To first order in these small parameters, Eq. (A9) can be written in the form

$$H_p^{(1)} \equiv \omega_c a^\dagger a + \sum_j \frac{\omega_j}{2} \sigma_j^z + \sum_j g_j \sigma_j^x \left(a + a^\dagger\right)$$
$$+ \sum_j 2\Omega_j \cos\left(\omega_j^d t + \phi_j\right) \sigma_j^x, \tag{A11}$$

where we have defined $\sigma_j^z \equiv |1\rangle_j \langle 1| - |0\rangle_j \langle 0|$ and the effective spin qubit frequencies $\omega_j \equiv \omega_{1,j} - \omega_{0,j} =$

$\left(\mathcal{W}_j - \mathcal{V}_j\right)/2$, $2\Omega_j \equiv \mathcal{F}_j \left|\sin\left(\Phi_j/2\right)\right|$ is the effective amplitude of the drive acting on the spin qubit, $g_j \equiv g_{c,j} \left|\sin\left(\Phi_j/2\right)\right|$ is the effective spin-photon coupling strength, and the sign of $\sin\left(\Phi_j/2\right)$ has been taken into account by making the replacement $\phi'_j \rightarrow \phi_j$ and redefining the phase of a accordingly in Eq. (A9). The Hamiltonian $H_p^{(1)}$ is identical in form to Eq. (2). Finally, we note that the Hamiltonian for DQD charge qubits [102] at the operation points $\epsilon_{0,j} = 0$ [described by setting $B_j^z = B_j^x = 0$ in Eq. (A2)] can also be written in a form analogous to Eq. (A11), with $\sigma_j^{z,x} \rightarrow \tau_j^{z,x}$, $\omega_j \rightarrow 2t_j$, $2\Omega_j \rightarrow \mathcal{F}_j$, and $g_j \rightarrow g_{c,j}$.

2. Three-electron resonant exchange qubits in triple quantum dots

We now consider two RX qubits, each defined by the spin states of three electrons in a triple quantum dot [66,67], that interact via a microwave cavity [68]. In contrast to one-electron spin qubits, each RX qubit couples directly to the electric field of microwave cavity photons via an intrinsic electric dipole moment. This dipole moment arises from the admixture of polarized charge states in the qubit states, without requiring spin-orbit coupling, magnetic gradients, or the fabrication of additional device elements such as micromagnets. The Hamiltonian given in Ref. [68, Eq. (29)], which is used to describe RX qubits coupled to a microwave cavity in the driven resonant regime, has the same general form as Eq. (2). Here, we briefly summarize the theory used to derive this Hamiltonian for RX qubits and adapt it to the case of silicon triple quantum dots.

An effective Hamiltonian for each RX qubit can be obtained from a Hubbard model for electrons confined within a linear triple quantum dot [67,68]. This model can be used to calculate a charge stability diagram (Ref. [67, Fig. 1(b)]) that describes the triple dot in terms of the lowest-energy charge configuration (n_1, n_2, n_3) (where n_i denotes the occupation number for dot i and the occupation numbers are ordered from the left dot to the right dot) as a function of the gate voltages applied to the three dots, which set the on-site energies $(-\varepsilon_1, -\varepsilon_2, -\varepsilon_3)$. For fixed $V_{\text{tot}} \equiv \sum_i \varepsilon_i$, the lowest-energy charge configuration depends on both the detuning $\epsilon \equiv \left(\varepsilon_3 - \varepsilon_1\right)/2$ and the relative middle dot on-site energy $V_m \equiv -\varepsilon_2 + \frac{1}{2}\left(\varepsilon_1 + \varepsilon_3\right)$. Distinct charge configurations are coupled via the left-center and center-right interdot tunneling amplitudes t_l and t_r, respectively.

References [67] and [68] consider a three-electron system in the subspace of the charge configurations $(1, 1, 1)$, $(2, 0, 1)$, and $(1, 0, 2)$. The relevant operation point is illustrated in Ref. [67, Fig. 1(b)]. Here, we focus on a silicon triple dot and assume that a sufficiently large ($\gtrsim 100$ mT [66]) static magnetic field is applied to the triple dot. Furthermore, we assume that excited valley states are well

separated in energy from the lowest-energy valley manifold (by a valley-splitting energy $E_V \gtrsim 100\,\mu\text{eV}$ [12,103–105]), such that a single-orbital picture is valid. We can then define a spin qubit using three-electron states in the lower-energy $S = 1/2$ spin subspace, which have a spin quantum number for the total z component $m_s = -1/2$ due to the positive electron g factor of silicon. The relevant subspace is spanned by the $(1, 1, 1)$ states

$$|e_0\rangle \equiv |s\rangle_{13}\,|\downarrow\rangle_2$$
$$= \frac{1}{\sqrt{2}}\left(c_{1\uparrow}^\dagger c_{2\downarrow}^\dagger c_{3\downarrow}^\dagger - c_{1\downarrow}^\dagger c_{2\downarrow}^\dagger c_{3\uparrow}^\dagger\right)|\text{vac}\rangle, \qquad \text{(A12)}$$

$$|g_0\rangle \equiv \sqrt{\frac{1}{3}}\,|t_0\rangle_{13}\,|\downarrow\rangle_2 - \sqrt{\frac{2}{3}}\,|t_-\rangle_{13}\,|\uparrow\rangle_2$$
$$= \frac{1}{\sqrt{6}}\left(c_{1\uparrow}^\dagger c_{2\downarrow}^\dagger c_{3\downarrow}^\dagger + c_{1\downarrow}^\dagger c_{2\downarrow}^\dagger c_{3\uparrow}^\dagger - 2c_{1\downarrow}^\dagger c_{2\uparrow}^\dagger c_{3\downarrow}^\dagger\right)|\text{vac}\rangle, \qquad \text{(A13)}$$

together with the $(2, 0, 1)$ and $(1, 0, 2)$ states

$$\left|s_{1,-1/2}\right\rangle \equiv |s\rangle_{11}\,|\downarrow\rangle_3 = c_{1\uparrow}^\dagger c_{1\downarrow}^\dagger c_{3\downarrow}^\dagger\,|\text{vac}\rangle, \qquad \text{(A14)}$$

$$\left|s_{3,-1/2}\right\rangle \equiv |\downarrow\rangle_1\,|s\rangle_{33} = c_{1\downarrow}^\dagger c_{3\uparrow}^\dagger c_{3\downarrow}^\dagger\,|\text{vac}\rangle, \qquad \text{(A15)}$$

where $|\text{vac}\rangle$ denotes the vacuum. In the basis $\{|e_0\rangle, |g_0\rangle, \left|s_{1,-1/2}\right\rangle, \left|s_{3,-1/2}\right\rangle\}$, the Hubbard Hamiltonian matrix has a form identical to that given in Ref. [67, Eq. (S7)] for the case $m_s = 1/2$.

The RX qubit is defined within an effective $(1, 0, 1)$ subspace $\left\{|\tilde{e_0}\rangle, |\tilde{g_0}\rangle\right\}$ obtained by perturbatively eliminating the $(2, 0, 1)$ and $(1, 0, 2)$ states via a Schrieffer-Wolff transformation [67,68]. The resulting effective Hamiltonian can be written in the form

$$H_{\text{eff}}^{(3)} = \frac{J}{2}\tilde{\sigma}^z - \frac{\sqrt{3}}{2}j\,\tilde{\sigma}^x, \qquad \text{(A16)}$$

where $\tilde{\sigma}^z \equiv |\tilde{e_0}\rangle\langle\tilde{e_0}| - |\tilde{g_0}\rangle\langle\tilde{g_0}|$, $J \equiv \left(J_l + J_r\right)/2$, $j \equiv \left(J_l - J_r\right)/2$, and the exchange between the center and left (right) dots is $J_l = t_l^2/\left(\Delta + \epsilon\right)$ $\left[J_r = t_r^2/\left(\Delta - \epsilon\right)\right]$. Here, Δ is defined in terms of Hubbard model parameters and V_m [67,68]. Diagonalizing $H_{\text{eff}}^{(3)}$ yields $H_0 = \omega\sigma^z/2$ with $\sigma^z \equiv |1\rangle\langle1| - |0\rangle\langle0|$, where the eigenstates $|0\rangle$ and $|1\rangle$ define the RX qubit and $\omega \equiv \sqrt{J^2 + 3j^2}$ is the qubit energy splitting (here, we set $\hbar = 1$). As the exchange interactions J_l and J_r between dots are controlled using only voltages applied to the triple quantum dot, the RX qubit is a spin qubit that can be fully manipulated using electric fields alone [66,67,106,107].

In addition to being fully controllable via dc electric field pulses, the RX qubit couples directly to microwave photons by virtue of the small admixture of the polarized charge states $(2, 0, 1)$ and $(1, 0, 2)$ in the logical qubit states [67,68]. This feature enables full resonant control of the RX qubit via electric fields, in direct analogy to resonant control of individual electronic and nuclear spins via magnetic fields in electron spin resonance (ESR) and nuclear magnetic resonance (NMR). The same charge admixture also enables coupling of the qubit to the electric field of photons in a microwave cavity, with a strength characterized by the charge admixture parameter $\xi \equiv t/\Delta$ (here, $t \equiv t_l = t_r$). The parameter ξ is a measure of the electric dipole moment of the qubit and is inversely proportional to Δ, which sets the width of the $(1, 1, 1)$ region and is tunable via V_m.

We can write the Hamiltonian for the RX qubit including electric dipole coupling as $H_{RX} = H_0 + H'_{int}$, where H'_{int} is the dipole interaction in the RX qubit basis. The operation point (ϵ_0, Δ_0) for the RX qubit determines the qubit frequency ω and the specific form of the electric dipole moment. Variations in both ϵ and Δ about this operation point enable coupling to microwave cavity photons [34,67,68,70,85] and are implemented via gate voltage control of the on-site energies $-\varepsilon_i$. Here, we focus on electric dipole coupling for small variations in the detuning ϵ [67,68]. For this case, the electric dipole moment of the RX qubit is along the triple-dot axis and can be described in terms of the operator $d = ew_0 (n_1 - n_3)/2$, where e is the magnitude of the electron charge and w_0 is the size of the triple dot (i.e., the distance between the centers of the outer dots). The operation point $\epsilon = \epsilon_0$ for the RX qubit is chosen such that the coupling to variations in the detuning ϵ [see, e.g., Eq. (1)] is perpendicular to the quantization axis of the RX qubit. In the basis of the RX qubit states, the dipole interaction of the triple dot with the fundamental cavity mode then takes the form [68]

$$H'_{int} = g\sigma^x \left(a + a^\dagger\right), \tag{A17}$$

where the effective qubit-photon coupling strength is given by

$$g = \frac{g_c}{2}\sqrt{(\partial_\epsilon J)^2 + 3\,(\partial_\epsilon j\,)^2}\bigg|_{\epsilon=\epsilon_0} \tag{A18}$$

and g_c is the charge-cavity coupling strength (an expression for g_c is derived from a circuit model in Ref. [68]). For the qubit operation point $\epsilon_0 = 0$ chosen in this work, $t_l = t_r \equiv t$ and $g = \sqrt{3}\xi^2 g_c/2$. Thus, maximizing ξ maximizes the coupling strength g.

In the driven resonant regime described in Ref. [68], two RX qubits interact with microwave cavity photons, the frequency of which we denote here as ω_c, in the presence of an external driving field of frequency $\omega^d \equiv \nu$ applied to

the cavity. A displacement transformation in the regime of large driving-field amplitude and large cavity-drive detuning $|\omega_c - \omega^d| \gg g, |\omega - \omega^d|$ then effectively transfers the drive from the cavity to the qubit and leads to Eq. (29) in Ref. [68] for each qubit. We can write this Hamiltonian for two RX qubits as

$$H_p^{(3)} = \omega_c a^\dagger a + \sum_j \frac{\omega_j}{2}\sigma_j^z + \sum_j g_j \sigma_j^x \left(a + a^\dagger\right)$$
$$+ \sum_j 2\Omega_j \cos\left(\omega_j^d t + \phi_j\right)\sigma_j^x, \tag{A19}$$

where we have redefined the phase ϕ_j to match the form of H_p in Eq. (2). We see that, like $H_p^{(1)}$ in Eq. (A11), $H_p^{(3)}$ has a form identical to H_p. We also note that this form for the Hamiltonian can be obtained for cavity-coupled RX qubits without a displacement transformation by directly driving the detuning of the RX qubits [66,67] as described by Eq. (1). Thus, the sideband-based interactions and associated entangling gates that we derive from H_p can be implemented using both RX qubits and one-electron spin qubits.

APPENDIX B: ONE-QUBIT SECOND-ORDER TERMS IN EFFECTIVE HAMILTONIAN

In this appendix, we analyze in more detail the one-qubit terms appearing at second order in the effective Hamiltonian $H_{eff}(\tau)$ [Eq. (16)], which originate from the commutators $\left[V_I, V'_I\right]_1$ and $\left[V_I, V'_I\right]_2$ defined in Eqs. (17) and (18). The one-qubit terms arising from $\left[V_I, V'_I\right]_1$ are given by

$$\Lambda_1 \equiv \frac{1}{2i\tau} \int_0^\tau dt \int_0^t dt' \left[V_I, V'_I\right]_1$$
$$= \frac{1}{2i\tau} \int_0^\tau dt \int_0^t dt' \sum_j \left\{\left[A_j, A'_j\right]a^{\dagger 2} + \left[A_j^\dagger, A_j'^\dagger\right]a^2\right.$$
$$\left. + \left(\left[A_j, A_j'^\dagger\right] + \left[A_j^\dagger, A'_j\right]\right)a^\dagger a\right\} \tag{B1}$$

and those arising from $\left[V_I, V'_I\right]_2$ are

$$\Lambda_2 \equiv \frac{1}{2i\tau} \int_0^\tau dt \int_0^t dt' \sum_j \left(A_j^\dagger A'_j - A_j'^\dagger A_j\right), \tag{B2}$$

where $A_j \equiv A_j(t)$ and $A'_j \equiv A_j(t')$. We note that the cavity-photon operators a and $a^\dagger$ appear in each term of Λ_1 but are absent from Λ_2.

Substituting for A_j and A'_j using Eq. (10) shows that evaluating the double integrals in Eqs. (B1) and (B2) amounts to evaluating double integrals of products of

exponentials of the form

$$h\left(\mu, \mu'\right) \equiv \frac{1}{2i\tau} \int_0^\tau dt \int_0^t dt'\, e^{-i\mu t} e^{i\mu' t'}$$

$$= \begin{cases} 0, & \mu \neq \mu' \\ -\frac{1}{2\mu} & \mu = \mu' \end{cases} \tag{B3}$$

or its complex conjugate $h^*\left(\mu, \mu'\right) = -h\left(-\mu, -\mu'\right)$. Here, $\mu, \mu' \in \{\pm \Delta_j, \pm\left(\Delta_j + W_j\right), \pm\left(\Delta_j - W_j\right)\}$. Since we set $\Delta_j = p_j \eta$ and $W_j = q_j \eta$ with integers p_j and q_j, we have $\mu_j = r_j \eta$ and $\mu'_j = r'_j \eta$ where r_j and r'_j are also integers. Equation (B1) then becomes

$$\Lambda_1 = \sum_j g_j^2 \left(\left\{ \sin\theta_j \sin^2\left(\frac{\theta_j}{2}\right) \left[h\left(-\Delta_j - W_j, \Delta_j\right) - h\left(-\Delta_j, \Delta_j + W_j\right)\right] \sigma_j^+ \right.\right.$$

$$+ \sin\theta_j \cos^2\left(\frac{\theta_j}{2}\right) \left[h\left(-\Delta_j + W_j, \Delta_j\right) - h\left(-\Delta_j, \Delta_j - W_j\right)\right] \sigma_j^-$$

$$\left. - \sin^2\left(\frac{\theta_j}{2}\right)\cos^2\left(\frac{\theta_j}{2}\right) \left[h\left(-\Delta_j - W_j, \Delta_j - W_j\right) - h\left(-\Delta_j + W_j, \Delta_j + W_j\right)\right] \sigma_j^z \right\} a^{\dagger 2}$$

$$+ \left\{ \left[\sin\theta_j \sin^2\left(\frac{\theta_j}{2}\right) h\left(-\Delta_j - W_j, -\Delta_j\right) + \sin\theta_j \cos^2\left(\frac{\theta_j}{2}\right) h\left(-\Delta_j, -\Delta_j + W_j\right)\right] \sigma_j^+ \right.$$

$$+ \left[\sin\theta_j \cos^2\left(\frac{\theta_j}{2}\right) h\left(-\Delta_j + W_j, -\Delta_j\right) + \sin\theta_j \sin^2\left(\frac{\theta_j}{2}\right) h\left(-\Delta_j, -\Delta_j - W_j\right)\right] \sigma_j^-$$

$$\left. + \left[\sin^4\left(\frac{\theta_j}{2}\right) h\left(-\Delta_j - W_j, -\Delta_j - W_j\right) - \cos^4\left(\frac{\theta_j}{2}\right) h\left(-\Delta_j + W_j, -\Delta_j + W_j\right)\right] \sigma_j^z \right\}$$

$$\times\, a^\dagger a + \text{H.c.} \right) \tag{B4}$$

and Eq. (B2) becomes

$$\Lambda_2 = -\sum_j \frac{g_j^2}{2} \left\{ \left[\sin\theta_j \sin^2\left(\frac{\theta_j}{2}\right) h\left(\Delta_j, \Delta_j + W_j\right) + \sin\theta_j \cos^2\left(\frac{\theta_j}{2}\right) h\left(\Delta_j - W_j, \Delta_j\right)\right] \sigma_+ \right.$$

$$+ \left[\sin\theta_j \sin^2\left(\frac{\theta_j}{2}\right) h\left(\Delta_j + W_j, \Delta_j\right) + \sin\theta_j \cos^2\left(\frac{\theta_j}{2}\right) h\left(\Delta_j, \Delta_j - W_j\right)\right] \sigma_-$$

$$\left. + \left[\sin^4\left(\frac{\theta_j}{2}\right) h\left(\Delta_j + W_j, \Delta_j + W_j\right) - \cos^4\left(\frac{\theta_j}{2}\right) h\left(\Delta_j - W_j, \Delta_j - W_j\right)\right] \sigma_z \right\}$$

$$+ \text{H.c.} \tag{B5}$$

In the above expressions for Λ_1 and Λ_2, we have dropped terms proportional to the identity operator that lead to global energy shifts. Using Eqs. (B4) and (B5) together with Eq. (B3), we can obtain the resonance conditions $\mu = \mu'$ under which $h\left(\mu, \mu'\right) \neq 0$ and particular one-qubit terms appear (i.e., are nonzero) in the effective Hamiltonian $H_{\text{eff}}(\tau)$. Note that these conditions are identical for $h\left(\mu, \mu'\right)$ and $h^*\left(\mu, \mu'\right)$.

The one-qubit resonance conditions and corresponding forms of the effective Hamiltonian terms are summarized in Table III. We see that the a^2 and $a^{\dagger 2}$ terms occur only

for $W_j = \left|2\Delta_j\right|$ or $\Delta_j = 0$. Assuming that we choose an operation point such that these conditions are not satisfied, the a^2 and $a^{\dagger 2}$ terms can be eliminated from the Hamiltonian. Additionally, the case $W_j = 0$ corresponds to a vanishing gap for dressed qubit j and thus does not have well-defined physical meaning. We can therefore also ignore the $\sigma_j^+ a^\dagger a$, $\sigma_j^- a^\dagger a$, σ_j^+, and σ_j^- terms. As a result, the only remaining one-qubit terms appearing at second order in the effective Hamiltonian are those of the form $\sigma_j^z a^\dagger a$ in Eq. (B4) and σ_j^z in Eq. (B5). These terms exist for any values of W_j and Δ_j. Finally, we note that Eq. (B3)

TABLE III. Resonance conditions for the appearance of specific one-qubit terms in the second-order effective Hamiltonian of Eq. (16).

Resonance condition	Hamiltonian terms
$W_j = 2\Delta_j$	$\sigma_j^+ a^2,\ \sigma_j^- a^{\dagger 2}$
$W_j = -2\Delta_j$	$\sigma_j^+ a^{\dagger 2},\ \sigma_j^- a^2$
$\Delta_j = 0$	$\sigma_j^z a^2,\ \sigma_j^z a^{\dagger 2}$
$W_j = 0$	$\sigma_j^+ a^\dagger a,\ \sigma_j^- a^\dagger a,\ \sigma_j^+,\ \sigma_j^-$
Any W_j, Δ_j	$\sigma_j^z a^\dagger a,\ \sigma_j^z$

is well defined only for $\mu, \mu' \neq 0$, which leads to the constraints $\Delta_j \neq 0$ and $W_j \neq |\Delta_j|$. The full one-qubit contribution to $H_{\text{eff}}(\tau)$ for $\Delta_j, W_j \neq 0$ and $W_j \neq |\Delta_j|, |2\Delta_j|$ is thus

$$\Lambda \equiv \Lambda_1 + \Lambda_2$$
$$= \sum_j g_j^2 \left[\frac{\sin^4\left(\frac{\theta_j}{2}\right)}{\Delta_j + W_j} - \frac{\cos^4\left(\frac{\theta_j}{2}\right)}{\Delta_j - W_j} \right] \sigma_j^z \left(a^\dagger a + \frac{1}{2} \right)$$
$$= -\sum_j g_j^2 \left[\frac{\delta_j^2 + 2\Delta_j \delta_j + W_j^2}{2W_j \left(\Delta_j^2 - W_j^2 \right)} \right] \sigma_j^z \left(a^\dagger a + \frac{1}{2} \right),$$
$$\tag{B6}$$

where we have used $\cos\theta_j = \delta_j / W_j$ [see Eq. (5)]. Equation (B6) represents the dispersive-shift terms induced by the parametric driving [88].

APPENDIX C: QUBIT-QUBIT INTERACTION TERMS IN EFFECTIVE HAMILTONIAN

The qubit-qubit interaction terms in $H_{\text{eff}}(\tau)$ [Eq. (16)], and therefore the generated two-qubit gates $U(\tau) \approx e^{-iH_{\text{eff}}\tau}$, are given by Eq. (21). Here, we derive the form of $V_{qq}(\tau)$ for each of the nine resonance conditions $\mu_1 = \mu_2$, where $\mu_1 \in \{\Delta_1, \Delta_1 + W_1, \Delta_1 - W_1\}$ and $\mu_2 \in \{\Delta_2, \Delta_2 + W_2, \Delta_2 - W_2\}$. As noted in the main text, these resonance conditions are obtained by substituting Eq. (10) into $V_{qq}(\tau)$, which yields terms with frequency differences $\mu_1 - \mu_2$, and subsequently applying Eq. (B3) to identify nonzero terms. In what follows, we use the abbreviated notation $\Delta_j^\pm \equiv \Delta_j \pm W_j$ and refer to the resonance conditions by the numbers given in Table I.

First, we consider the resonance condition $\Delta_1 = \Delta_2$ (resonance condition 1), which is equivalent to $\omega_1^d = \omega_2^d$ and therefore describes the driving of both qubits at the same frequency. In order to select a specific form for the two-qubit interaction, we also assume that the constraints $W_1 \neq \pm W_2$ are satisfied so that terms in $V_{qq}(\tau)$ with $\mu_1 - \mu_2 \neq \Delta_1 - \Delta_2$ remain nonzero and vanish according to Eq. (B3). In terms of the resonant detuning $\Delta \equiv \Delta_1 = \Delta_2$,

we find that Eq. (21) becomes

$$V_{qq}(\tau) = \frac{g_1 g_2}{4} [2h(\Delta, \Delta) - 2h(-\Delta, -\Delta)]$$
$$\times \sin\theta_1 \sin\theta_2 \sigma_1^z \sigma_2^z$$
$$= -\frac{g_1 g_2}{2\Delta} \sin\theta_1 \sin\theta_2 \sigma_1^z \sigma_2^z$$
$$= -2\mathcal{J} \sin\theta_1 \sin\theta_2 \sigma_1^z \sigma_2^z, \tag{C1}$$

where we have defined $\mathcal{J} \equiv g_1 g_2 / 4\Delta$. For resonant qubit driving such that $\delta_1 = \delta_2 = 0$, $W_1 = 2\Omega_1$, $W_2 = 2\Omega_2$, and $\sin\theta_1 = \sin\theta_2 = 1$. In this case, $\Delta_1 = \Delta_2$ corresponds to $\omega_1 = \omega_2$. In other words, since the detunings of both qubit frequencies from the cavity frequency ω_c are aligned, the center frequencies of the driven qubits are also resonant. Equation (C1) then reduces to

$$V_{qq}(\tau) = -2\mathcal{J}\sigma_1^z \sigma_2^z, \tag{C2}$$

which can be used to generate a controlled-phase gate (see Appendix D).

In a similar way, we can derive the form of the two-qubit interaction and corresponding constraints for each of the remaining resonance conditions. Resonance condition 2 (3), given by $\Delta_1 = \Delta_2^+$ ($\Delta_1 = \Delta_2^-$), is equivalent to $\omega_1^d = \omega_2^d - W_2$ ($\omega_1^d = \omega_2^d + W_2$). For $\Delta \equiv \Delta_1 = \Delta_2^\pm$, we find

$$V_{qq}(\tau) = \mp \frac{g_1 g_2}{4} [h(\Delta, \Delta) - h(-\Delta, -\Delta)]$$
$$\times \sin\theta_1 (1 \mp \cos\theta_2) \sigma_1^z \sigma_2^x$$
$$= \pm \mathcal{J} \sin\theta_1 (1 \mp \cos\theta_2) \sigma_1^z \sigma_2^x, \tag{C3}$$

with the same set of constraints $W_1 \neq \pm W_2, \pm 2W_2$ for each resonance condition. In the case of resonant qubit driving, the resonance condition $\Delta_1 = \Delta_2^+$ ($\Delta_1 = \Delta_2^-$) corresponds to $\omega_1 = \omega_2 - 2\Omega_2$ ($\omega_1 = \omega_2 + 2\Omega_2$) such that the center frequency of qubit 1 is aligned with the red (blue) sideband of qubit 2. In this case, $\sin\theta_1 = 1$ and $\cos\theta_2 = 0$, which reduces Eq. (C3) to

$$V_{qq}(\tau) = \pm \mathcal{J}\sigma_1^z \sigma_2^x \tag{C4}$$

for $\Delta_1 = \Delta_2^\pm$.

The resonance conditions $\Delta_1^+ = \Delta_2$ and $\Delta_1^- = \Delta_2$ (resonance conditions 4 and 5) describe cases in which the roles of qubits 1 and 2 are reversed relative to $\Delta_1 = \Delta_2^+$ and $\Delta_1 = \Delta_2^-$, respectively. Accordingly, $\Delta_1^+ = \Delta_2$ ($\Delta_1^- = \Delta_2$) is equivalent to $\omega_1^d - W_1 = \omega_2^d$ ($\omega_1^d + W_1 = \omega_2^d$) and the qubit-qubit interaction takes the form

$$V_{qq}(\tau) = \pm \mathcal{J}(1 \mp \cos\theta_1) \sin\theta_2 \sigma_1^x \sigma_2^z \tag{C5}$$

for $\Delta \equiv \Delta_1^\pm = \Delta_2$ and constraints such that $W_1 \leftrightarrow W_2$ relative to the constraints for resonance conditions 2 and 3.

In the case of resonantly driven qubits, $\Delta_1^+ = \Delta_2$ ($\Delta_1^- = \Delta_2$) corresponds to $\omega_1 - 2\Omega_1 = \omega_2$ ($\omega_1 + 2\Omega_1 = \omega_2$) so that the center frequency of qubit 2 is aligned with the red (blue) sideband of qubit 1, and Eq. (C5) becomes

$$V_{qq}(\tau) = \pm \mathcal{J}\sigma_1^x \sigma_2^z \qquad (C6)$$

for $\Delta_1^\pm = \Delta_2$.

We next consider the resonance conditions $\Delta_1^+ = \Delta_2^+$ and $\Delta_1^- = \Delta_2^-$ (resonance conditions 6 and 7), which are equivalent to $\omega_1^d - W_1 = \omega_2^d - W_2$ and $\omega_1^d + W_1 = \omega_2^d + W_2$, respectively. The form of the effective qubit-qubit interaction for $\Delta \equiv \Delta_1^\pm = \Delta_2^\pm$ is

$$V_{qq}(\tau) = -\mathcal{J}(1 \mp \cos\theta_1)(1 \mp \cos\theta_2)(\sigma_1^+ \sigma_2^- + \sigma_1^- \sigma_2^+), \qquad (C7)$$

with an identical set of constraints $W_1 \neq W_2, 2W_2, W_2/2$ for each resonance condition. For resonant driving of both qubits, $\Delta_1^+ = \Delta_2^+$ ($\Delta_1^- = \Delta_2^-$) corresponds to $\omega_1 - 2\Omega_1 = \omega_2 - 2\Omega_2$ ($\omega_1 + 2\Omega_1 = \omega_2 + 2\Omega_2$) such that the red (blue) sidebands of both qubits are in resonance, and Eq. (C7) becomes

$$V_{qq}(\tau) = -\mathcal{J}(\sigma_1^+ \sigma_2^- + \sigma_1^- \sigma_2^+) \qquad (C8)$$

for both $\Delta = \Delta_1^+ = \Delta_2^+$ and $\Delta = \Delta_1^- = \Delta_2^-$.

Finally, the resonance conditions $\Delta_1^- = \Delta_2^-$ and $\Delta_1^- = \Delta_2^+$ (resonance conditions 8 and 9) are equivalent to $\omega_1^d - W_1 = \omega_2^d + W_2$ and $\omega_1^d + W_1 = \omega_2^d - W_2$, respectively. The effective qubit-qubit interaction for $\Delta \equiv \Delta_1^\pm = \Delta_2^\mp$ takes the form

$$V_{qq}(\tau) = \mathcal{J}(1 \mp \cos\theta_1)(1 \pm \cos\theta_2)(\sigma_1^+ \sigma_2^+ + \sigma_1^- \sigma_2^-), \qquad (C9)$$

again with an identical set of constraints $W_1 \neq -W_2, -2W_2, -W_2/2$ for each resonance condition. Note that, for the physically relevant case $W_{1,2} > 0$, these constraints are always satisfied. For resonant driving of both qubits, $\Delta_1^+ = \Delta_2^-$ ($\Delta_1^- = \Delta_2^+$) corresponds to $\omega_1 - 2\Omega_1 = \omega_2 + 2\Omega_2$ ($\omega_1 + 2\Omega_1 = \omega_2 - 2\Omega_2$), such that the red (blue) sideband of qubit 1 is in resonance with the blue (red) sideband of qubit 2. Equation (C9) becomes

$$V_{qq}(\tau) = \mathcal{J}(\sigma_1^+ \sigma_2^+ + \sigma_1^- \sigma_2^-) \qquad (C10)$$

for both $\Delta = \Delta_1^+ = \Delta_2^-$ and $\Delta = \Delta_1^- = \Delta_2^+$.

The above nine resonance conditions, their associated constraints, and the corresponding forms of the effective qubit-qubit interaction $V_{qq}(\tau)$ for resonant qubit driving are summarized in Table I of the main text.

APPENDIX D: ELIMINATION OF DRIVE-INDUCED DISPERSIVE-SHIFT DYNAMICS FROM EFFECTIVE HAMILTONIAN

As shown in Appendix B, the parametric drive-induced dispersive-shift terms Λ [Eq. (B6)] in general exist for any W_j and Δ_j (provided that $W_j \neq |\Delta_j|$). Nevertheless, it is possible to effectively eliminate the dynamics generated by Λ in specific cases by appropriately choosing parameters and operation times such that the gate in the presence of Λ is equivalent to that for $\Lambda = 0$. Here, we first illustrate this method for the resonant qubit driving case $\delta_j = 0$ and the resonance conditions 7 and 9 in Table I and Fig. 2. We then consider the effects of Λ for additional resonance conditions, as well as the off-resonant qubit driving case $\delta_j \neq 0$, for which we can choose parameters such that $\Lambda = 0$.

We first consider resonant qubit driving, described by $\delta_j = 0$ such that $W_j = 2\Omega_j$, $\Lambda = \Lambda_r$, and $\chi_j \neq 0$. From Eqs. (16), (20), and (21), the effective Hamiltonian for $\Delta_j = p_j \eta$ and $W_j = q_j \eta$ with p_j, q_j integers, $\Delta_j, W_j \neq 0$, and $W_j \neq |\Delta_j|, |2\Delta_j|$ is given by

$$H_{\text{eff}}(\tau) = \lambda^2 \bar{H}_2(\tau)$$
$$= V_{qq}(\tau) + \Lambda_r. \qquad (D1)$$

As discussed in the main text, the desired ideal two-qubit evolution is generated by the qubit-qubit interaction term V_{qq} according to $U_m \equiv e^{-iV_{qq}\tau_m}$, where $\tau_m \equiv m\tau = 2\pi m/\eta$ is the corresponding gate time. We now also define an evolution operator with the dispersive-shift terms included as $U_m' \equiv e^{-iH_{\text{eff}}\tau_m}$, where H_{eff} is given by Eq. (D1).

From Eq. (21), we note that V_{qq} is independent of photon operators $a, a^\dagger$. We also see from Eq. (20) that Λ_r is diagonal in the photon number n. We can therefore write

$$\Lambda_r = \sum_n \Lambda_n, \qquad (D2)$$

where $\Lambda_n \equiv P_n \Lambda_r P_n = \langle n| \Lambda_r |n\rangle P_n$ is the operator describing the dispersive-shift terms within the n-photon subspace and $P_n \equiv |n\rangle \langle n|$ is the corresponding subspace projector, and work in a subspace of fixed n. Noting that $V_{qq}(\tau)$ consists only of qubit operators [see Eq. (21)], we find $H_{\text{eff}}^{(n)} \equiv P_n H_{\text{eff}} P_n = P_n (V_{qq} + \Lambda_r) P_n = V_{qq} + \Lambda_n$, where we now use V_{qq} to denote the n-photon subspace operator. In the basis $\{|ee,n\rangle, |eg,n\rangle, |ge,n\rangle, |gg,n\rangle\}$, Λ_n takes the form

$$\Lambda_n = \left(n + \frac{1}{2}\right) \begin{pmatrix} \chi_1 + \chi_2 & & & \\ & \chi_1 - \chi_2 & & \\ & & -\chi_1 + \chi_2 & \\ & & & -\chi_1 - \chi_2 \end{pmatrix}, \qquad (D3)$$

while the form of V_{qq} depends on the particular resonance condition according to Table I. The evolution

with the dispersive-shift terms included is described by $P_n U'_m P_n = e^{-iH_{\text{eff}}^{(n)} \tau_m} = e^{-i(V_{qq}+\Lambda_n)\tau_m}$. As in the main text, we use U_m and U'_m to denote the evolution operators within the n-photon two-qubit subspace and suppress the photon-number state $|n\rangle$ in what follows.

We first consider resonance condition 7, which is defined by $\Delta \equiv \Delta_1^- = \Delta_2^-$. In the main text, we have noted that the ideal evolution within the n-photon subspace can be written as $U_m = e^{i\mathcal{J}\tau_m \Sigma_x}$, where $\Sigma_x \equiv |eg\rangle\langle ge| + |ge\rangle\langle eg|$. The ideal operation U_m therefore acts nontrivially only within the two-dimensional subspace $\{|eg\rangle, |ge\rangle\}$, and Σ_x has an action analogous to the Pauli operator σ_x in this subspace.

From Eq. (D3) and the form of V_{qq} for resonance condition 7 [Eq. (C8)], we find that $H_{\text{eff}}^{(n)}$ is block diagonal. In this case, we can write $H_{\text{eff}}^{(n)} = P H_{\text{eff}}^{(n)} P + Q H_{\text{eff}}^{(n)} Q$, where we have defined the two-qubit subspace projectors

$$P \equiv |ee\rangle\langle ee| + |gg\rangle\langle gg|,$$
$$Q \equiv |eg\rangle\langle eg| + |ge\rangle\langle ge|. \tag{D4}$$

We can then characterize the effect of Λ_n on the dynamics for a given initial state $|\psi_i\rangle$ via a fidelity

$$
\begin{aligned}
F_s &\equiv \left| \langle\psi_i| U_m^\dagger U'_m |\psi_i\rangle \right|^2 \\
&= \left| \langle\psi_i| P \left(P U_m^\dagger P\right) \left(P U'_m P\right) P |\psi_i\rangle \right. \\
&\quad \left. + \langle\psi_i| Q \left(Q U_m^\dagger Q\right) \left(Q U'_m Q\right) Q |\psi_i\rangle \right|^2,
\end{aligned} \tag{D5}
$$

where we have used $U_m = P U_m P + Q U_m Q$ and $U'_m = P U'_m P + Q U'_m Q$.

For resonance condition 7, we find

$$P H_{\text{eff}}^{(n)} P = \left(n + \frac{1}{2}\right)(\chi_1 + \chi_2)\Sigma'_z,$$

$$Q H_{\text{eff}}^{(n)} Q = \left(n + \frac{1}{2}\right)(\chi_1 - \chi_2)\Sigma_z - \mathcal{J}\Sigma_x, \tag{D6}$$

where we have defined the operators $\Sigma_z \equiv |eg\rangle\langle eg| - |ge\rangle\langle ge|$ and $\Sigma'_z \equiv |ee\rangle\langle ee| - |gg\rangle\langle gg|$ in analogy to the Pauli operator σ_z. For an initial state $|\psi_i\rangle$ in the subspace associated with Q, evolution for $\Lambda_n \neq 0$ remains within this space such that $U'_m |\psi_i\rangle = Q U'_m Q |\psi_i\rangle$. In the main text, we consider the initial state $|\psi_i\rangle = |eg\rangle$. For the iSWAP gate $U_{i\text{sw}}$, which is equivalent to U_m at time $\tau_m = \pi/2\mathcal{J}$ [see Eq. (22)], the ideal final state is $|\psi_f\rangle = U_{i\text{sw}}|\psi_i\rangle = U_{i\text{sw}}|eg\rangle = i|ge\rangle$.

We now set $n = 0$ for simplicity [in what follows, generalization of the expressions to any n using Eq. (D3) is straightforward and amounts to the replacements $(\chi_1 \pm \chi_2)/2 \rightarrow \left(n + \frac{1}{2}\right)(\chi_1 \pm \chi_2)$]. In the presence of Λ_0 and defining the unit vector $\hat{\mathbf{u}} \equiv \left[(\chi_1 - \chi_2)\hat{z} - 2\mathcal{J}\hat{x}\right]/\tilde{\Omega}$

with $\tilde{\Omega} \equiv \sqrt{(\chi_1 - \chi_2)^2 + 4\mathcal{J}^2}$, the action of the gate is modified to

$$
\begin{aligned}
QU'_m Q |\psi_i\rangle &= e^{-i\frac{\tilde{\Omega}\tau_m}{2}\hat{\mathbf{u}}\cdot\boldsymbol{\Sigma}} |eg\rangle \\
&= \left[\cos\left(\frac{\tilde{\Omega}\tau_m}{2}\right) - i\sin\left(\frac{\tilde{\Omega}\tau_m}{2}\right)\left(\frac{\chi_1 - \chi_2}{\tilde{\Omega}}\right)\right] \\
&\quad \times |eg\rangle + i\sin\left(\frac{\tilde{\Omega}\tau_m}{2}\right)\left(\frac{2\mathcal{J}}{\tilde{\Omega}}\right)|ge\rangle. \tag{D7}
\end{aligned}
$$

Using Eqs. (D5) and (D7) along with $P U_m P |\psi_i\rangle = P U'_m P |\psi_i\rangle = 0$, we find

$$
\begin{aligned}
F_s &= \left| \langle\psi_i| Q \left(Q U_m^\dagger Q\right)\left(Q U'_m Q\right) Q |\psi_i\rangle \right|^2 \\
&= \frac{4\mathcal{J}^2}{\tilde{\Omega}^2}\sin^2\left(\frac{\tilde{\Omega}\tau_m}{2}\right), \tag{D8}
\end{aligned}
$$

which oscillates with the modified frequency $\tilde{\Omega}$ instead of $\mathcal{J}$ in the ideal case. Nevertheless, we can recover the ideal dynamics and obtain $F_s = 1$ for the iSWAP gate time $\tau_m = \pi/2\mathcal{J}$ by choosing parameters for which $\chi_1 = \chi_2$, such that $Q H_{\text{eff}}^{(n)} Q = V_{qq}$ and $Q U'_m Q = Q U_m Q$. The constraints that must be satisfied by the parameters for resonance condition 7 (in addition to those listed in Table I) are therefore (a) $\tau_m = \pi/2\mathcal{J}$, (b) $\chi_1 = \chi_2$, and (c) $w \equiv p_1 - q_1 = p_2 - q_2$ from the resonance condition itself. From constraint (a) and using $\Delta = w\eta$, we find $\tau_m \equiv 2\pi m/\eta = \pi/2\mathcal{J} = 2\pi w\eta/g_1 g_2$, or

$$g_1 g_2 = \frac{w}{m}\eta^2, \tag{D9}$$

while constraint (b) becomes, using Eq. (20) with $\Delta_j = p_j\eta$, $W_j = 2\Omega_j = q_j\eta$, and $\Delta = \Delta_1^- = \Delta_2^- = w\eta$ and incorporating constraint (c),

$$\frac{g_2^2}{g_1^2} = \frac{2 + \frac{w}{q_2}}{2 + \frac{w}{q_1}}. \tag{D10}$$

We also note that q_1, q_2, p_1, p_2, w, and m must all be integers.

There are multiple sets of parameter values that satisfy these constraints, and we choose one set (given in Table II) for the fidelity analysis described in this work. To show that this approach effectively restores the ideal iSWAP evolution in the absence of the dispersive-shift terms, we choose $n = 0$ and compare the ideal state at time τ_m for $\Lambda_r = 0$ with the numerical solution to the time-dependent Schrödinger equation for the density matrix in the interaction picture, $\dot{\rho}_I = -i[V_I, \rho_I]$, for V_I given by Eq. (9), the initial state $\rho_I(0) = |\psi_i\rangle\langle\psi_i| = |eg, 0\rangle\langle eg, 0|$, and the chosen set of parameters. For the numerical calculations,

we work in the photon subspace with $n = 0, 1, 2$. The ideal final state is given by

$$
\begin{aligned}
\rho_I^f (\tau_m) &= |\psi_f\rangle\langle\psi_f| \\
&= U_{i\mathrm{SW}} \rho_I (0) U_{i\mathrm{SW}}^\dagger \\
&= |ge, 0\rangle \langle ge, 0| .
\end{aligned}
\tag{D11}
$$

For the comparison, we calculate the fidelity [91]

$$
F_0 (\tau_m) \equiv \mathrm{Tr}\left[\rho_I^f (\tau_m) \rho_I^{(0)} (\tau_m) \right],
\tag{D12}
$$

where $\rho_I^{(0)} (\tau_m)$ denotes the numerical solution in the absence of decay, i.e., for $\gamma_j = \kappa = 0$ in the master equation of Eq. (25). For the chosen parameters, we find $F_0 \approx 0.998$, confirming that setting $\chi_1 = \chi_2$ effectively eliminates the modification to the dynamics induced by the dispersive-shift terms Λ_r and restores the evolution expected for the iSWAP gate.

We now apply this approach to resonance condition 9, which from Table I is given by $\Delta \equiv \Delta_1^- = \Delta_2^+$. From the form of V_{qq} [Eq. (C10)], the effective Hamiltonian for this case is again block-diagonal and can be written as $H_{\mathrm{eff}}^{(n)} = P H_{\mathrm{eff}}^{(n)} P + Q H_{\mathrm{eff}}^{(n)} Q$. As described in the main text, ideal evolution within the n-photon subspace can be expressed as $U_m = e^{-i\mathcal{J}\tau_m \Sigma_x'}$, where $\Sigma_x' \equiv |ee\rangle\langle gg| + |gg\rangle\langle ee|$. The ideal evolution in this case occurs nontrivially only within the two-dimensional subspace associated with P in Eq. (D4), and we find that

$$
PH_{\mathrm{eff}}^{(n)}P = \left(n + \frac{1}{2}\right)(\chi_1 + \chi_2)\Sigma_z' + \mathcal{J}\Sigma_x',
$$

$$
QH_{\mathrm{eff}}^{(n)}Q = \left(n + \frac{1}{2}\right)(\chi_1 - \chi_2)\Sigma_z.
\tag{D13}
$$

If we now assume that the initial state $|\psi_i\rangle$ lies within the subspace associated with P, evolution for $\Lambda_n \neq 0$ remains within this space such that $U_m' |\psi_i\rangle = PU_m'P |\psi_i\rangle$. Here, we consider the initial state $|\psi_i\rangle = |ee\rangle$. For the double-excitation gate $U_{i\mathrm{DE}}$ described in the main text, which is equivalent to U_m at time $\tau_m = -\pi/2\mathcal{J}$ [see Eq. (23)] the ideal final state is $|\psi_f\rangle = U_{i\mathrm{DE}} |\psi_i\rangle = U_{i\mathrm{DE}} |ee\rangle = i |gg\rangle$.

Again, we set $n = 0$ for simplicity [with straightforward generalization of expressions to any n via $(\chi_1 \pm \chi_2)/2 \rightarrow \left(n + \frac{1}{2}\right)(\chi_1 \pm \chi_2)$]. In terms of $\hat{\mathbf{u}}' \equiv \left[(\chi_1 + \chi_2)\hat{z} + 2\mathcal{J}\hat{x}\right]/\Omega'$ with $\Omega' \equiv \sqrt{(\chi_1 + \chi_2)^2 + 4\mathcal{J}^2}$, the modified action of the gate in the presence of Λ_0 is

given by

$$
\begin{aligned}
PU_m'P |\psi_i\rangle &= e^{-i\frac{\Omega'\tau_m}{2}\hat{\mathbf{u}}'\cdot\mathbf{\Sigma}'} |ee\rangle \\
&= \left[\cos\left(\frac{\Omega'\tau_m}{2}\right) - i\sin\left(\frac{\Omega'\tau_m}{2}\right)\left(\frac{\chi_1 + \chi_2}{\Omega'}\right)\right] \\
&\quad \times |ee\rangle - i\sin\left(\frac{\Omega'\tau_m}{2}\right)\left(\frac{2\mathcal{J}}{\Omega'}\right) |gg\rangle .
\end{aligned}
\tag{D14}
$$

Since $QU_mQ |\psi_i\rangle = QU_m'Q |\psi_i\rangle = 0$, Eq. (D5) then reduces to

$$
\begin{aligned}
F_s &= \left| \langle\psi_i| P \left(PU_m^\dagger P\right)\left(PU_m'P\right) P |\psi_i\rangle \right|^2 \\
&= \frac{4\mathcal{J}^2}{\Omega'^2} \sin^2\left(\frac{\Omega'\tau_m}{2}\right).
\end{aligned}
\tag{D15}
$$

F_s now oscillates with the modified frequency Ω' instead of $\mathcal{J}$ in the ideal case. We can again recover the ideal dynamics and obtain $F_s = 1$ for the gate time $\tau_m = -\pi/2\mathcal{J}$ by choosing parameters such that $\chi_1 = -\chi_2$, which yields $PH_{\mathrm{eff}}^{(n)}P = V_{qq}$ and $PU_m'P = PU_mP$. Thus, the constraints that must be satisfied by the parameters for resonance condition 9 (in addition to those listed in Table I) are (a) $\tau_m = -\pi/2\mathcal{J}$, (b) $\chi_1 = -\chi_2$, and (c) $w \equiv p_1 - q_1 = p_2 + q_2$ from the resonance condition. From constraint (a) and using $\Delta = w\eta$, we find $\tau_m \equiv 2\pi m/\eta = -\pi/2\mathcal{J} = -2\pi w\eta/g_1g_2$, which gives

$$
g_1g_2 = -\frac{w}{m}\eta^2.
\tag{D16}
$$

On the other hand, constraint (b) with constraint (c) incorporated becomes [again using Eq. (20) with $\Delta_j = p_j\eta$, $W_j = 2\Omega_j = q_j\eta$, and $\Delta = \Delta_1^- = \Delta_2^+ = w\eta$],

$$
\frac{g_2^2}{g_1^2} = \frac{2 - \frac{w}{q_2}}{2 + \frac{w}{q_1}}.
\tag{D17}
$$

As before, q_1, q_2, p_1, p_2, w, and m must all be integers.

There are once again multiple sets of parameter values that satisfy these constraints, and we choose one set (given in Table II) for the analysis described in this work. We now show that the ideal evolution described by $U_{i\mathrm{DE}}$ in the absence of the dispersive-shift terms is restored for $\chi_1 = -\chi_2$ and the chosen parameters. Working in the photon subspace with $n = 0, 1, 2$ and numerically solving $\dot{\rho}_I = -i[V_I, \rho_I]$ for resonance condition 9 with the initial state $\rho_I (0) = |\psi_i\rangle \langle\psi_i| = |ee, 0\rangle \langle ee, 0|$, we compare the $\gamma_j = \kappa = 0$ solution $\rho_I^{(0)} (\tau_m)$ at time τ_m with the ideal

($\Lambda_r = 0$) final state

$$
\begin{aligned}
\rho_I^f(\tau_m) &= |\psi_f\rangle\langle\psi_f| \\
&= U_{i\mathrm{DE}}\rho_I(0)U_{i\mathrm{DE}}^\dagger \\
&= |gg,0\rangle\langle gg,0|
\end{aligned}
\tag{D18}
$$

via the fidelity in Eq. (D12). We find $F_0 \approx 0.998$, showing that setting $\chi_1 = -\chi_2$ effectively eliminates the modification to the dynamics induced by the dispersive-shift terms and restores the expected gate evolution generated by V_{qq} for resonance condition 9. The small error $1 - F_0$ found for both resonance conditions 7 and 9 also serves as a measure of the validity of the model that we develop in this work.

By choosing parameters that satisfy additional constraints, a similar approach can be used to eliminate dispersive-shift dynamics for general initial states $|\psi_i\rangle$ with arbitrary photon number n, as well as for other resonance conditions and the corresponding interactions and two-qubit gates listed in Table I. For a general initial state

$$
|\psi_i\rangle = c_{ee}|ee,n\rangle + c_{eg}|eg,n\rangle + c_{ge}|ge,n\rangle + c_{gg}|gg,n\rangle,
\tag{D19}
$$

both the subspaces associated with P and Q must be taken into account. For resonance condition 7, we find

$$
\begin{aligned}
PU_m'P|\psi_i\rangle &= Pe^{-i\Lambda_n\tau_m}P \\
&= e^{-i\left(n+\frac{1}{2}\right)(\chi_1+\chi_2)\tau_m}|ee,n\rangle\langle ee,n| \\
&\quad + e^{i\left(n+\frac{1}{2}\right)(\chi_1+\chi_2)\tau_m}|gg,n\rangle\langle gg,n|
\end{aligned}
\tag{D20}
$$

and $PU_mP|\psi_i\rangle = P|\psi_i\rangle$, while for resonance condition 9,

$$
\begin{aligned}
QU_m'Q|\psi_i\rangle &= Qe^{-i\Lambda_n\tau_m}Q \\
&= e^{-i\left(n+\frac{1}{2}\right)(\chi_1-\chi_2)\tau_m}|eg,n\rangle\langle eg,n| \\
&\quad + e^{i\left(n+\frac{1}{2}\right)(\chi_1-\chi_2)\tau_m}|ge,n\rangle\langle ge,n|
\end{aligned}
\tag{D21}
$$

and $QU_mQ|\psi_i\rangle = Q|\psi_i\rangle$. From the forms of Eqs. (D20) and (D21), we see that setting $\chi_j = 2\pi k_j$ with k_j an integer for $j = 1, 2$, along with $k_1 = k_2$ ($k_1 = -k_2$) for resonance condition 7 (9) to satisfy $\chi_1 = \chi_2$ ($\chi_1 = -\chi_2$) eliminates the dynamical phases due to Λ_r and restores the ideal evolution due to V_{qq} within a subspace of fixed n, or for an integer average photon number $\langle a^\dagger a\rangle$.

We now consider the other resonance conditions in Table I. Resonance condition 1 is given by $\Delta \equiv \Delta_1 = \Delta_2$ and (assuming that the associated constraints listed in the table are satisfied by W_1 and W_2) yields $V_{qq} = -2\mathcal{J}\sigma_1^z\sigma_2^z$. This interaction is equivalent to that which generates a Mølmer-Sørensen gate in the original qubit basis [108] and can be used to construct a controlled-phase gate

in the dressed-qubit basis considered here. Using $U_m = e^{-iV_{qq}\tau_m} = e^{i2\mathcal{J}\tau_m\sigma_1^z\sigma_2^z}$, a sequence for a controlled-phase gate is given by

$$
\begin{aligned}
U_\varphi &= e^{i2\mathcal{J}\tau_m}e^{-i2\mathcal{J}\tau_m\sigma_1^z}e^{-i2\mathcal{J}\tau_m\sigma_2^z}U_m \\
&= \begin{pmatrix} 1 & & & \\ & 1 & & \\ & & 1 & \\ & & & e^{i\varphi} \end{pmatrix},
\end{aligned}
\tag{D22}
$$

where $\varphi \equiv 8\mathcal{J}\tau_m$, which shows that U_m for $\Delta \equiv \Delta_1 = \Delta_2$ is equivalent to a controlled-phase gate up to single-qubit rotations. For $\varphi = (2l+1)\pi$ or $\tau_m = (2l+1)\pi/8\mathcal{J}$ with l an integer, U_φ represents a controlled-Z gate U_{CZ}.

To determine conditions for eliminating the dispersive-shift dynamics in the case of resonance condition 1, we can compare the action of U_m and $U_m' = e^{-i(V_{qq}+\Lambda_n)\tau_m} = e^{-i\Lambda_n\tau_m}U_m$, both of which now act in the full two-qubit space, on a general state $|\psi_i\rangle$ in this space [Eq. (D19)] via

$$
\begin{aligned}
F_s &= \left|\langle\psi_i|U_m^\dagger U_m'|\psi_i\rangle\right|^2 \\
&= \left|\langle\psi_i|e^{-i\Lambda_n\tau_m}|\psi_i\rangle\right|^2 \\
&= \left| |c_{ee}|^2 e^{-i\left(n+\frac{1}{2}\right)(\chi_1+\chi_2)\tau_m} + |c_{eg}|^2 e^{-i\left(n+\frac{1}{2}\right)(\chi_1-\chi_2)\tau_m} \right. \\
&\quad \left. + |c_{ge}|^2 e^{i\left(n+\frac{1}{2}\right)(\chi_1-\chi_2)\tau_m} + |c_{gg}|^2 e^{i\left(n+\frac{1}{2}\right)(\chi_1+\chi_2)\tau_m} \right|^2.
\end{aligned}
\tag{D23}
$$

In this case, we can in principle recover the ideal dynamics and obtain $F_s = 1$ for any state $|\psi_i\rangle$ by choosing parameters that satisfy $\chi_j = 2\pi k_j$ with k_j an integer for $j = 1, 2$ and that also satisfy $\tau_m = \varphi/8\mathcal{J}$, $p_1 = p_2$ from the resonance condition, and $q_1 \neq \pm q_2$ from Table I to obtain a controlled-phase gate U_φ according to the construction in Eq. (D22). For U_{CZ}, $\tau_m = (2l+1)\pi/8\mathcal{J}$, and we can proceed to identify potential parameter sets by choosing, e.g., $l = 0$ and setting $\tau_m \equiv 2\pi m/\eta = \pi/8\mathcal{J}$ in analogy to the analysis described above for resonance conditions 7 and 9.

The remaining physically distinct case in Table I is that of resonance condition 4, given by $\Delta \equiv \Delta_1^+ = \Delta_2$ and corresponding to $V_{qq} = \mathcal{J}\sigma_1^x\sigma_2^z$ when W_1 and W_2 satisfy the listed constraints. This interaction can be used to construct a controlled-NOT (CNOT) gate [45]. We note that V_{qq}, and therefore U_m and U_m', are block diagonal with the associated subspace projectors $P' = |ee\rangle\langle ee| + |ge\rangle\langle ge|$ and $Q' = |eg\rangle\langle eg| + |gg\rangle\langle gg|$. If we choose $|\psi_i\rangle = |eg\rangle$ such that $P'U_mP'|\psi_i\rangle = P'U_m'P'|\psi_i\rangle = 0$, we find from a calculation similar to that in Eqs. (D5) and (D8),

$$
\begin{aligned}
F_s &= \left|\langle\psi_i|U_m^\dagger U_m'|\psi_i\rangle\right|^2 \\
&= \frac{4\mathcal{J}^2}{\bar{\Omega}^2}\sin^2\left(\frac{\bar{\Omega}\tau_m}{2}\right)
\end{aligned}
\tag{D24}
$$

with $\bar{\Omega} \equiv \sqrt{\chi_1 + 4\mathcal{J}^2}$. In this case, recovering the dynamics for $\Lambda_r = 0$ requires $\chi_1 = 0$, which is not possible for $\delta_j = 0$ and $g_1, 2\Omega_1 \neq 0$ [see Eq. (20)]. Similar results hold for other initial states $|\psi_i\rangle$. While $F_s = 1$ is not achievable exactly for resonance condition 4 when $\delta_j = 0$, choosing appropriate parameters to minimize χ_j in principle allows F_s to be made arbitrarily close to unity, enabling the dynamics for $\Lambda_r = 0$ and thus the gate generated by $V_{qq} = \mathcal{J}\sigma_1^x\sigma_2^z$ to be well approximated. The dispersive-shift dynamics can also be eliminated in this case for $\delta_j \neq 0$, as we describe below. The other resonance conditions in Table I lead to effective interactions V_{qq} that are either identical in form to those considered above or have the roles of qubits 1 and 2 reversed.

Finally, we consider the conditions under which the one-qubit contribution to $H_{\text{eff}}(\tau)$, including the dispersive-shift terms Λ, can be made to vanish for each qubit individually. In this case, $H_{\text{eff}}(\tau) = V_{qq}(\tau)$ consists solely of qubit-qubit interaction terms. Setting $\Lambda = 0$ in Eq. (19) yields the condition $\delta_j^2 + 2\Delta_j\delta_j + W_j^2 = 0$ or, equivalently, $\delta_j^2 + 2p_j\eta\delta_j + q_j^2\eta^2 = 0$. We note that for resonant driving, described by $\delta_j = 0$, the one-qubit contribution $\Lambda \neq 0$ unless $W_j = 0$, which is not physically meaningful (see Appendix B). Thus, provided that the drive frequency is not on resonance with the qubit frequency $\left(\omega_j^d \neq \omega_j\right)$, the dispersive-shift terms can be eliminated individually for each qubit by an appropriate choice of parameters.

We note that dynamical phase errors due to the drive-induced dispersive-shift terms, as well as any additional dispersive shifts arising at higher orders in the Magnus expansion, could potentially also be compensated via a time-dependent qubit-drive detuning [109,110] implemented by modulating either the amplitude or frequency (via, e.g., a linearly chirped drive frequency) in time. While this approach may partially reduce the parameter constraints we describe, it also imposes additional temporal requirements on the control fields needed during operation of the gates. Here, we have presented an alternative approach that relies on appropriately fixed parameter values. Detailed analysis and optimization of control methods for correcting these phase shifts are left for future work.

---

[1] D. P. DiVincenzo, The physical implementation of quantum computation, Fortschr. Phys. **48**, 771 (2000).

[2] T. D. Ladd, F. Jelezko, R. Laflamme, Y. Nakamura, C. Monroe, and J. L. O'Brien, Quantum computers, Nature **464**, 45 (2010).

[3] J. M. Taylor, H. A. Engel, W. Dur, A. Yacoby, C. M. Marcus, P. Zoller, and M. D. Lukin, Fault-tolerant architecture for quantum computation using electrically controlled semiconductor spins, Nat. Phys. **1**, 177 (2005).

[4] L. Jiang, J. M. Taylor, A. S. Sørensen, and M. D. Lukin, Distributed quantum computation based on small quantum registers, Phys. Rev. A **76**, 062323 (2007).

[5] C. Monroe, R. Raussendorf, A. Ruthven, K. R. Brown, P. Maunz, L.-M. Duan, and J. Kim, Large-scale modular quantum-computer architecture with atomic memory and photonic interconnects, Phys. Rev. A **89**, 022317 (2014).

[6] L. M. K. Vandersypen, H. Bluhm, J. S. Clarke, A. S. Dzurak, R. Ishihara, A. Morello, D. J. Reilly, L. R. Schreiber, and M. Veldhorst, Interfacing spin qubits in quantum dots and donors—hot, dense, and coherent, npj Quantum Inf. **3**, 34 (2017).

[7] G. Tosi, F. A. Mohiyaddin, V. Schmitt, S. Tenberg, R. Rahman, G. Klimeck, and A. Morello, Silicon quantum processor with robust long-distance qubit couplings, Nat. Commun. **8**, 450 (2017).

[8] H. Jnane, B. Undseth, Z. Cai, S. C. Benjamin, and B. Koczor, Multicore quantum computing, Phys. Rev. Appl. **18**, 044064 (2022).

[9] D. Loss and D. P. DiVincenzo, Quantum computation with quantum dots, Phys. Rev. A **57**, 120 (1998).

[10] B. E. Kane, A silicon-based nuclear spin quantum computer, Nature **393**, 133 (1998).

[11] R. Hanson, L. P. Kouwenhoven, J. R. Petta, S. Tarucha, and L. M. K. Vandersypen, Spins in few-electron quantum dots, Rev. Mod. Phys. **79**, 1217 (2007).

[12] F. A. Zwanenburg, A. S. Dzurak, A. Morello, M. Y. Simmons, L. C. L. Hollenberg, G. Klimeck, S. Rogge, S. N. Coppersmith, and M. A. Eriksson, Silicon quantum electronics, Rev. Mod. Phys. **85**, 961 (2013).

[13] L. Petit, H. G. J. Eenink, M. Russ, W. I. L. Lawrie, N. W. Hendrickx, S. G. J. Philips, J. S. Clarke, L. M. K. Vandersypen, and M. Veldhorst, Universal quantum logic in hot silicon qubits, Nature **580**, 355 (2020).

[14] A. Chatterjee, P. Stevenson, S. De Franceschi, A. Morello, N. P. de Leon, and F. Kuemmeth, Semiconductor qubits in practice, Nat. Rev. Phys. **3**, 157 (2021).

[15] A. Noiri, K. Takeda, T. Nakajima, T. Kobayashi, A. Sammak, G. Scappucci, and S. Tarucha, Fast universal quantum gate above the fault-tolerance threshold in silicon, Nature **601**, 338 (2022).

[16] X. Xue, M. Russ, N. Samkharadze, B. Undseth, A. Sammak, G. Scappucci, and L. M. K. Vandersypen, Quantum logic with spin qubits crossing the surface code threshold, Nature **601**, 343 (2022).

[17] A. R. Mills, C. R. Guinn, M. J. Gullans, A. J. Sigillito, M. M. Feldman, E. Nielsen, and J. R. Petta, Two-qubit silicon quantum processor with operation fidelity exceeding 99%, Sci. Adv. **8**, eabn5130 (2022).

[18] A. J. Weinstein, *et al.*, Universal logic with encoded spin qubits in silicon, Nature **615**, 817 (2023).

[19] G. Burkard, T. D. Ladd, A. Pan, J. M. Nichol, and J. R. Petta, Semiconductor spin qubits, Rev. Mod. Phys. **95**, 025003 (2023).

[20] L. Childress, A. S. Sørensen, and M. D. Lukin, Mesoscopic cavity quantum electrodynamics with quantum dots, Phys. Rev. A **69**, 042302 (2004).

[21] A. Blais, R.-S. Huang, A. Wallraff, S. M. Girvin, and R. J. Schoelkopf, Cavity quantum electrodynamics for superconducting electrical circuits: An architecture for quantum computation, Phys. Rev. A **69**, 062320 (2004).

[22] A. Wallraff, D. I. Schuster, A. Blais, L. Frunzio, R. S. Huang, J. Majer, S. Kumar, S. M. Girvin, and R. J. Schoelkopf, Strong coupling of a single photon to a superconducting qubit using circuit quantum electrodynamics, Nature **431**, 162 (2004).

[23] A. Blais, J. Gambetta, A. Wallraff, D. I. Schuster, S. M. Girvin, M. H. Devoret, and R. J. Schoelkopf, Quantum-information processing with circuit quantum electrodynamics, Phys. Rev. A **75**, 032329 (2007).

[24] J. Majer, J. M. Chow, J. M. Gambetta, J. Koch, B. R. Johnson, J. A. Schreier, L. Frunzio, D. I. Schuster, A. A. Houck, A. Wallraff, A. Blais, M. H. Devoret, S. M. Girvin, and R. J. Schoelkopf, Coupling superconducting qubits via a cavity bus, Nature **449**, 443 (2007).

[25] M. A. Sillanpää, J. I. Park, and R. W. Simmonds, Coherent quantum state storage and transfer between two phase qubits via a resonant cavity, Nature **449**, 438 (2007).

[26] A. Blais, A. L. Grimsmo, S. M. Girvin, and A. Wallraff, Circuit quantum electrodynamics, Rev. Mod. Phys. **93**, 025005 (2021).

[27] A. A. Clerk, K. W. Lehnert, P. Bertet, J. R. Petta, and Y. Nakamura, Hybrid quantum systems with circuit quantum electrodynamics, Nat. Phys. **16**, 257 (2020).

[28] G. Burkard, M. J. Gullans, X. Mi, and J. R. Petta, Superconductor-semiconductor hybrid-circuit quantum electrodynamics, Nat. Rev. Phys. **2**, 129 (2020).

[29] M. Veldhorst, J. C. C. Hwang, C. H. Yang, A. W. Leenstra, B. de Ronde, J. P. Dehollain, J. T. Muhonen, F. E. Hudson, K. M. Itoh, A. Morello, and A. S. Dzurak, An addressable quantum dot qubit with fault-tolerant control-fidelity, Nat. Nanotechnol. **9**, 981 (2014).

[30] M. Veldhorst, C. H. Yang, J. C. C. Hwang, W. Huang, J. P. Dehollain, J. T. Muhonen, S. Simmons, A. Laucht, F. E. Hudson, K. M. Itoh, A. Morello, and A. S. Dzurak, A two-qubit logic gate in silicon, Nature **526**, 410 (2015).

[31] J. Yoneda, K. Takeda, T. Otsuka, T. Nakajima, M. R. Delbecq, G. Allison, T. Honda, T. Kodera, S. Oda, Y. Hoshi, N. Usami, K. M. Itoh, and S. Tarucha, A quantum-dot spin qubit with coherence limited by charge noise and fidelity higher than 99.9%, Nat. Nanotechnol. **13**, 102 (2018).

[32] X. Mi, M. Benito, S. Putz, D. M. Zajac, J. M. Taylor, G. Burkard, and J. R. Petta, A coherent spin-photon interface in silicon, Nature **555**, 599 (2018).

[33] N. Samkharadze, G. Zheng, N. Kalhor, D. Brousse, A. Sammak, U. C. Mendes, A. Blais, G. Scappucci, and L. M. K. Vandersypen, Strong spin-photon coupling in silicon, Science **359**, 1123 (2018).

[34] A. J. Landig, J. V. Koski, P. Scarlino, U. C. Mendes, A. Blais, C. Reichl, W. Wegscheider, A. Wallraff, K. Ensslin, and T. Ihn, Coherent spin-photon coupling using a resonant exchange qubit, Nature **560**, 179 (2018).

[35] A. J. Landig, J. V. Koski, P. Scarlino, C. Müller, J. C. Abadillo-Uriel, B. Kratochwil, C. Reichl, W. Wegscheider, S. N. Coppersmith, M. Friesen, A. Wallraff, T. Ihn, and K. Ensslin, Virtual-photon-mediated spin-qubit–transmon coupling, Nat. Commun. **10**, 5037 (2019).

[36] C. X. Yu, S. Zihlmann, J. C. Abadillo-Uriel, V. P. Michal, N. Rambal, H. Niebojewski, T. Bedecarrats, M. Vinet, É. Dumur, M. Filippone, B. Bertrand, S. De Franceschi, Y.-M. Niquet, and R. Maurand, Strong coupling between a photon and a hole spin in silicon, Nat. Nanotechnol. **18**, 741 (2023).

[37] F. Borjans, X. G. Croot, X. Mi, M. J. Gullans, and J. R. Petta, Resonant microwave-mediated interactions between distant electron spins, Nature **577**, 195 (2020).

[38] P. Harvey-Collard, J. Dijkema, G. Zheng, A. Sammak, G. Scappucci, and L. M. K. Vandersypen, Coherent spin-spin coupling mediated by virtual microwave photons, Phys. Rev. X **12**, 021026 (2022).

[39] M. Benito, J. R. Petta, and G. Burkard, Optimized cavity-mediated dispersive two-qubit gates between spin qubits, Phys. Rev. B **100**, 081412 (2019).

[40] A. Warren, E. Barnes, and S. E. Economou, Long-distance entangling gates between quantum dot spins mediated by a superconducting resonator, Phys. Rev. B **100**, 161303 (R) (2019).

[41] C. Rigetti, A. Blais, and M. Devoret, Protocol for universal gates in optimally biased superconducting qubits, Phys. Rev. Lett. **94**, 240502 (2005).

[42] A. Wallraff, D. I. Schuster, A. Blais, J. M. Gambetta, J. Schreier, L. Frunzio, M. H. Devoret, S. M. Girvin, and R. J. Schoelkopf, Sideband transitions and two-tone spectroscopy of a superconducting qubit strongly coupled to an on-chip cavity, Phys. Rev. Lett. **99**, 050501 (2007).

[43] P. J. Leek, S. Filipp, P. Maurer, M. Baur, R. Bianchetti, J. M. Fink, M. Göppl, L. Steffen, and A. Wallraff, Using sideband transitions for two-qubit operations in superconducting circuits, Phys. Rev. B **79**, 180511 (2009).

[44] C. Rigetti and M. Devoret, Fully microwave-tunable universal gates in superconducting qubits with linear couplings and fixed transition frequencies, Phys. Rev. B **81**, 134507 (2010).

[45] J. M. Chow, A. D. Córcoles, J. M. Gambetta, C. Rigetti, B. R. Johnson, J. A. Smolin, J. R. Rozen, G. A. Keefe, M. B. Rothwell, M. B. Ketchen, and M. Steffen, Simple all-microwave entangling gate for fixed-frequency superconducting qubits, Phys. Rev. Lett. **107**, 080502 (2011).

[46] F. Beaudoin, M. P. da Silva, Z. Dutton, and A. Blais, First-order sidebands in circuit QED using qubit frequency modulation, Phys. Rev. A **86**, 022305 (2012).

[47] D. C. McKay, S. Filipp, A. Mezzacapo, E. Magesan, J. M. Chow, and J. M. Gambetta, Universal gate for fixed-frequency qubits via a tunable bus, Phys. Rev. Appl. **6**, 064007 (2016).

[48] G. Tosi, F. A. Mohiyaddin, S. Tenberg, A. Laucht, and A. Morello, Robust electric dipole transition at microwave frequencies for nuclear spin qubits in silicon, Phys. Rev. B **98**, 075313 (2018).

[49] A. J. Sigillito, M. J. Gullans, L. F. Edge, M. Borselli, and J. R. Petta, Coherent transfer of quantum information in a silicon double quantum dot using resonant SWAP gates, npj Quantum Inf. **5**, 110 (2019).

[50] R. Ruskov and C. Tahan, Modulated longitudinal gates on encoded spin qubits via curvature couplings to a superconducting cavity, Phys. Rev. B **103**, 035301 (2021).

[51] A. Warren, U. Güngördü, J. P. Kestner, E. Barnes, and S. E. Economou, Robust photon-mediated entangling gates between quantum dot spin qubits, Phys. Rev. B **104**, 115308 (2021).

[52] I. Hansen, A. E. Seedhouse, A. Saraiva, A. Laucht, A. S. Dzurak, and C. H. Yang, Pulse engineering of a global field for robust and universal quantum computation, Phys. Rev. A **104**, 062415 (2021).

[53] S. R. McMillan and G. Burkard, Resonant direct CNOT in remote double quantum dot spin qubits, Phys. Rev. B **108**, 125414 (2023).

[54] J. Mielke and G. Burkard, Dispersive cavity-mediated quantum gate between driven dot-donor nuclear spins, Phys. Rev. B **107**, 155302 (2023).

[55] P. Bertet, C. J. P. M. Harmans, and J. E. Mooij, Parametric coupling for superconducting qubits, Phys. Rev. B **73**, 064512 (2006).

[56] A. O. Niskanen, Y. Nakamura, and J.-S. Tsai, Tunable coupling scheme for flux qubits at the optimal point, Phys. Rev. B **73**, 094506 (2006).

[57] A. O. Niskanen, K. Harrabi, F. Yoshihara, Y. Nakamura, S. Lloyd, and J. S. Tsai, Quantum coherent tunable coupling of superconducting qubits, Science **316**, 723 (2007).

[58] M. Reagor, *et al.*, Demonstration of universal parametric entangling gates on a multi-qubit lattice, Sci. Adv. **4**, eaao3603 (2018).

[59] N. Didier, E. A. Sete, M. P. da Silva, and C. Rigetti, Analytical modeling of parametrically modulated transmon qubits, Phys. Rev. A **97**, 022330 (2018).

[60] J. A. Valery, S. Chowdhury, G. Jones, and N. Didier, Dynamical sweet spot engineering via two-tone flux modulation of superconducting qubits, PRX Quantum **3**, 020337 (2022).

[61] A. Petrescu, C. Le Calonnec, C. Leroux, A. Di Paolo, P. Mundada, S. Sussman, A. Vrajitoarea, A. A. Houck, and A. Blais, Accurate methods for the analysis of strong-drive effects in parametric gates, Phys. Rev. Appl. **19**, 044003 (2023).

[62] B. R. Mollow, Power spectrum of light scattered by two-level systems, Phys. Rev. **188**, 1969 (1969).

[63] H. Kim, T. C. Shen, K. Roy-Choudhury, G. S. Solomon, and E. Waks, Resonant interactions between a Mollow triplet sideband and a strongly coupled cavity, Phys. Rev. Lett. **113**, 027403 (2014).

[64] M. Benito, X. Mi, J. M. Taylor, J. R. Petta, and G. Burkard, Input-output theory for spin-photon coupling in Si double quantum dots, Phys. Rev. B **96**, 235434 (2017).

[65] X. Croot, X. Mi, S. Putz, M. Benito, F. Borjans, G. Burkard, and J. R. Petta, Flopping-mode electric dipole spin resonance, Phys. Rev. Res. **2**, 012006 (2020).

[66] J. Medford, J. Beil, J. M. Taylor, E. I. Rashba, H. Lu, A. C. Gossard, and C. M. Marcus, Quantum-dot-based resonant exchange qubit, Phys. Rev. Lett. **111**, 050501 (2013).

[67] J. M. Taylor, V. Srinivasa, and J. Medford, Electrically protected resonant exchange qubits in triple quantum dots, Phys. Rev. Lett. **111**, 050502 (2013).

[68] V. Srinivasa, J. M. Taylor, and C. Tahan, Entangling distant resonant exchange qubits via circuit quantum electrodynamics, Phys. Rev. B **94**, 205421 (2016).

[69] J. C. Abadillo-Uriel, C. King, S. N. Coppersmith, and M. Friesen, Long-range two-hybrid-qubit gates mediated by a microwave cavity with red sidebands, Phys. Rev. A **104**, 032612 (2021).

[70] M. Russ and G. Burkard, Long distance coupling of resonant exchange qubits, Phys. Rev. B **92**, 205412 (2015).

[71] J. Levy, Universal quantum computation with spin-1/2 pairs and Heisenberg exchange, Phys. Rev. Lett. **89**, 147902 (2002).

[72] J. R. Petta, A. C. Johnson, J. M. Taylor, E. A. Laird, A. Yacoby, M. D. Lukin, C. M. Marcus, M. P. Hanson, and A. C. Gossard, Coherent manipulation of coupled electron spins in semiconductor quantum dots, Science **309**, 2180 (2005).

[73] G. Burkard and A. Imamoglu, Ultra-long-distance interaction between spin qubits, Phys. Rev. B **74**, 041307 (2006).

[74] J. M. Taylor and M. D. Lukin, Cavity quantum electrodynamics with semiconductor double-dot molecules on a chip, arXiv:cond-mat/0605144 (2006).

[75] J. M. Taylor, J. R. Petta, A. C. Johnson, A. Yacoby, C. M. Marcus, and M. D. Lukin, Relaxation, dephasing, and quantum control of electron spins in double quantum dots, Phys. Rev. B **76**, 035315 (2007).

[76] C. G. L. Bøttcher, S. P. Harvey, S. Fallahi, G. C. Gardner, M. J. Manfra, U. Vool, S. D. Bartlett, and A. Yacoby, Parametric longitudinal coupling between a high-impedance superconducting resonator and a semiconductor quantum dot singlet-triplet spin qubit, Nat. Commun. **13**, 4773 (2022).

[77] J. Corrigan *et al.*, Longitudinal coupling between a $Si/Si_{1-x}Ge_x$ double quantum dot and an off-chip TiN resonator, Phys. Rev. Appl. **20**, 064005 (2023).

[78] G. Scappucci, C. Kloeffel, F. A. Zwanenburg, D. Loss, M. Myronov, J.-J. Zhang, S. De Franceschi, G. Katsaros, and M. Veldhorst, The germanium quantum information route, Nat. Rev. Mater. **6**, 926 (2021).

[79] M. Benito, X. Croot, C. Adelsberger, S. Putz, X. Mi, J. R. Petta, and G. Burkard, Electric-field control and noise protection of the flopping-mode spin qubit, Phys. Rev. B **100**, 125430 (2019).

[80] J. Koch, T. M. Yu, J. Gambetta, A. A. Houck, D. I. Schuster, J. Majer, A. Blais, M. H. Devoret, S. M. Girvin, and R. J. Schoelkopf, Charge-insensitive qubit design derived from the Cooper pair box, Phys. Rev. A **76**, 042319 (2007).

[81] A. A. Houck, J. Koch, M. H. Devoret, S. M. Girvin, and R. J. Schoelkopf, Life after charge noise: Recent results with transmon qubits, Quantum Inf. Process. **8**, 105 (2009).

[82] J. Fei, J.-T. Hung, T. S. Koh, Y.-P. Shim, S. N. Coppersmith, X. Hu, and M. Friesen, Characterizing gate operations near the sweet spot of an exchange-only qubit, Phys. Rev. B **91**, 205434 (2015).

[83] M. Russ and G. Burkard, Asymmetric resonant exchange qubit under the influence of electrical noise, Phys. Rev. B **91**, 235411 (2015).

[84] Y.-P. Shim and C. Tahan, Charge-noise-insensitive gate operations for always-on exchange-only qubits, Phys. Rev. B **93**, 121410 (R) (2016).

[85] M. Russ, F. Ginzel, and G. Burkard, Coupling of three-spin qubits to their electric environment, Phys. Rev. B **94**, 165411 (2016).

[86] W. Magnus, On the exponential solution of differential equations for a linear operator, Commun. Pure Appl. Math. **7**, 649 (1954).

[87] A. M. Childs and I. L. Chuang, Universal quantum computation with two-level trapped ions, Phys. Rev. A **63**, 012306 (2000).

[88] T. Noh, Z. Xiao, X. Y. Jin, K. Cicak, E. Doucet, J. Aumentado, L. C. G. Govia, L. Ranzani, A. Kamal, and R. W. Simmonds, Strong parametric dispersive shifts in a statically decoupled two-qubit cavity QED system, Nat. Phys. **19**, 1445 (2023).

[89] N. Schuch and J. Siewert, Natural two-qubit gate for quantum computation using the XY interaction, Phys. Rev. A **67**, 032301 (2003).

[90] M. McEwen, D. Bacon, and C. Gidney, Relaxing hardware requirements for surface code circuits using time-dynamics, Quantum **7**, 1172 (2023).

[91] L. M. K. Vandersypen and I. L. Chuang, NMR techniques for quantum control and computation, Rev. Mod. Phys. **76**, 1037 (2005).

[92] J. M. Gambetta, F. Motzoi, S. T. Merkel, and F. K. Wilhelm, Analytic control methods for high-fidelity unitary operations in a weakly nonlinear oscillator, Phys. Rev. A **83**, 012308 (2011).

[93] M. Werninghaus, D. J. Egger, F. Roy, S. Machnes, F. K. Wilhelm, and S. Filipp, Leakage reduction in fast superconducting qubit gates via optimal control, npj Quantum Inf. **7**, 14 (2021).

[94] A. Plathanam Babu, J. Tuorila, and T. Ala-Nissila, State leakage during fast decay and control of a superconducting transmon qubit, npj Quantum Inf. **7**, 30 (2021).

[95] V. E. Manucharyan, J. Koch, L. I. Glazman, and M. H. Devoret, Fluxonium: Single Cooper-pair circuit free of charge offsets, Science **326**, 113 (2009).

[96] G. Zhu, D. G. Ferguson, V. E. Manucharyan, and J. Koch, Circuit QED with fluxonium qubits: Theory of the dispersive regime, Phys. Rev. B **87**, 024510 (2013).

[97] L. B. Nguyen, Y.-H. Lin, A. Somoroff, R. Mencia, N. Grabon, and V. E. Manucharyan, High-coherence fluxonium qubit, Phys. Rev. X **9**, 041041 (2019).

[98] F. Bao, *et al.*, Fluxonium: An alternative qubit platform for high-fidelity operations, Phys. Rev. Lett. **129**, 010502 (2022).

[99] L. Ding, M. Hays, Y. Sung, B. Kannan, J. An, A. Di Paolo, A. H. Karamlou, T. M. Hazard, K. Azar, D. K. Kim, B. M. Niedzielski, A. Melville, M. E. Schwartz, J. L. Yoder, T. P. Orlando, S. Gustavsson, J. A. Grover, K. Serniak, and W. D. Oliver, High-fidelity, frequency-flexible two-qubit fluxonium gates with a transmon coupler, Phys. Rev. X **13**, 031035 (2023).

[100] X. Zhang, Z. Zhu, N. P. Ong, and J. R. Petta, High-impedance superconducting resonators and on-chip filters for circuit quantum electrodynamics with semiconductor quantum dots, Phys. Rev. Appl. **21**, 014019 (2024).

[101] V. Srinivasa, K. C. Nowack, M. Shafiei, L. M. K. Vandersypen, and J. M. Taylor, Simultaneous spin-charge relaxation in double quantum dots, Phys. Rev. Lett. **110**, 196803 (2013).

[102] K. D. Petersson, J. R. Petta, H. Lu, and A. C. Gossard, Quantum coherence in a one-electron semiconductor charge qubit, Phys. Rev. Lett. **105**, 246804 (2010).

[103] C. H. Yang, A. Rossi, R. Ruskov, N. S. Lai, F. A. Mohiyaddin, S. Lee, C. Tahan, G. Klimeck, A. Morello, and A. S. Dzurak, Spin-valley lifetimes in a silicon quantum dot with tunable valley splitting, Nat. Commun. **4**, 2069 (2013).

[104] A. Hollmann, T. Struck, V. Langrock, A. Schmidbauer, F. Schauer, T. Leonhardt, K. Sawano, H. Riemann, N. V. Abrosimov, D. Bougeard, and L. R. Schreiber, Large, tunable valley splitting and single-spin relaxation mechanisms in a Si/Si$_x$Ge$_{1-x}$ quantum dot, Phys. Rev. Appl. **13**, 034068 (2020).

[105] T. McJunkin, B. Harpt, Y. Feng, M. P. Losert, R. Rahman, J. P. Dodson, M. A. Wolfe, D. E. Savage, M. G. Lagally, S. N. Coppersmith, M. Friesen, R. Joynt, and M. A. Eriksson, SiGe quantum wells with oscillating Ge concentrations for quantum dot qubits, Nat. Commun. **13**, 7777 (2022).

[106] D. P. DiVincenzo, D. Bacon, J. Kempe, G. Burkard, and K. B. Whaley, Universal quantum computation with the exchange interaction, Nature **408**, 339 (2000).

[107] J. Medford, J. Beil, J. M. Taylor, S. D. Bartlett, A. C. Doherty, E. I. Rashba, D. P. DiVincenzo, H. Lu, A. C. Gossard, and C. M. Marcus, Self-consistent measurement and state tomography of an exchange-only spin qubit, Nat. Nanotechnol. **8**, 654 (2013).

[108] A. Sørensen and K. Mølmer, Quantum computation with ions in thermal motion, Phys. Rev. Lett. **82**, 1971 (1999).

[109] F. Motzoi, J. M. Gambetta, P. Rebentrost, and F. K. Wilhelm, Simple pulses for elimination of leakage in weakly nonlinear qubits, Phys. Rev. Lett. **103**, 110501 (2009).

[110] A. Di Paolo, C. Leroux, T. M. Hazard, K. Serniak, S. Gustavsson, A. Blais, and W. D. Oliver, Extensible circuit-QED architecture via amplitude- and frequency-variable microwaves, arXiv:2204.08098 (2022).

Correction: The value given in the seventeenth row of the last column of Table II was incorrect and has been fixed.